中图分类号：V474

论文编号：10006LS1925202

北京航空航天大學

硕士学位论文

刚柔耦合小卫星的动力学与控制研究

作者姓名　派瑞加

学科专业　航空宇航科学与技术(空间技术应用)

指导教师　孙亮

培养院系　国际学院

Dynamics and Control of Rigid-flexible Coupling Microsatellite

A Dissertation Submitted for the Degree of Master

Candidate: Josue Manuel Pareja Contreras

Supervisor: Prof. Sun Liang

International School

Beihang University, Beijing, China

中图分类号：V474

论文编号：10006LS1925202

硕 士 学 位 论 文

刚柔耦合小卫星的动力学与控制研究

作者姓名: 派瑞加　　申请学位级别　工学硕士

指导教师姓名: 孙亮　　职称： 教授

学科专业: 航空宇航科学与技术(空间技术应用)　　研究方向 小卫星技术

学习时间自 2019 年 9 月 15 日　　起至 2021 年 06 月 日止

论文提交日期 2021 年 5 月 20 日　　论文答辩日期 2021 年 06 月 04 日

学位授予单位　北京航空航天大学　　学位授予日期　　年　月　日

关于学位论文的独创性声明

本人郑重声明：所呈交的论文是本人在指导教师指导下独立进行研究工作所取得的成果，论文中有关资料和数据是实事求是的。尽我所知，除文中已经加以标注和致谢外，本论文不包含其他人已经发表或撰写的研究成果，也不包含本人或他人为获得北京航空航天大学或其它教育机构的学位或学历证书而使用过的材料。与我一同工作的同志对研究所做的任何贡献均已在论文中作出了明确的说明。

若有不实之处，本人愿意承担相关法律责任。

学位论文作者签名：  日期： 2021 年 05 月 21 日

学位论文使用授权书

本人完全同意北京航空航天大学有权使用本学位论文（包括但不限于其印刷版和电子版），使用方式包括但不限于：保留学位论文，按规定向国家有关部门（机构）送交学位论文，以学术交流为目的赠送和交换学位论文，允许学位论文被查阅、借阅和复印，将学位论文的全部或部分内容编入有关数据库进行检索，采用影印、缩印或其他复制手段保存学位论文。

保密学位论文在解密后的使用授权同上。

学位论文作者签名：  日期： 2021 年 05 月 21 日

指导教师签名：  日期： 2021 年 6 月 8 日

摘 要

APSCO-SSS 项目由亚太空间合作组织(APSCO)发起。该项目由 1 颗微小卫星(SSS-1)和 2 颗立方体卫星(SSS-2A 和 SSS-2B)组成，用于盘绕式伸展臂展开技术、ADS-B 技术和遥感技术的空间验证。在本项目中，微小卫星 SSS-1 是由主星和子星通过一个盘绕式伸展臂连接组成的刚柔多体耦合系统。盘绕式伸展臂的柔性振动给微小卫星的控制带来了很大的困难和挑战。

首先利用 Lagrange 方法建立刚柔耦合微小卫星的数学模型。在动力学方面，通常将盘绕式伸展臂看作是一种柔性附件，并将其简化为欧拉-伯努利梁来做处理。但是在 SSS-1 卫星盘绕式伸展臂的末端配备了一个大质量部件(子星)， 因此和之前的处理方法不同，在推导动力学方程时必须考虑刚性子星的存在。

然后将卫星看作三轴旋转物体，其上的柔性附件会受到横向变形的影响，本文不考虑轴向变形和扭转变形。将整个系统的动能作为拉格朗日过程的自然步骤导出，这包括从三个卫星元件（刚性主卫星、柔性盘绕式伸展臂和刚性子卫星）获得的动能。为了简化系统的总动能表达式，采用了一些矩阵符号，用假定模态法可以得到整个系统的质量矩阵。通过定义系统的势能，采用假定模态法进行离散，得到了模型的刚度矩阵和阻尼矩阵。

本文不考虑卫星姿态以较大速率、较大角度的旋转，因此柔性附件的横向变形较小。在这个基础上，可以将得到的动态对象线性化，从而进一步合成一个线性控制器，用于直接的姿态控制和振动抑制。在动态被控对象的闭环控制中，设计出两个控制器：第一个是 H_∞控制器，其主要作用是使外源输入(w)转化到调节输出(z)时的影响最小。为此，从 w 到 z 的传递函数 LFT 的范数也必须最小；第二个是 μ 自适应前馈控制器，与第一个控制器相比，该方法能够在推导出鲁棒控制器的同时考虑系统的参数不确定性。

最后，在控制策略方面，动态被控对象与不同的加权函数相互关联，可以将某些任务优先于其他任务。本文所设计控制系统的首要任务是将整个卫星结构控制在期望的方向上，然后系统的重点是抑制柔性附件的振动。至于所需传感器数据，系统将使用三个方向的欧拉角和盘绕式伸展臂一端的附属物（子星）的横向加速度。分别在卫星标称和不确定条件下，比较从两个合成控制器获得的结果。

关键词：动力学，拉格朗日，机械振动，鲁棒控制

Abstract

The APSCO-SSS project is initiated by the Asia-Pacific Space Cooperation Organization (APSCO). This project consists of 1 micro-satellite (SSS-1) and 2 cube-satellites (SSS-2A and SSS-2B) implemented for different objectives such as: demonstration of coilable mast deployment, ADS-B technology and remote sensing. In this project, the micro-satellite SSS-1 is formed by a main-satellite and a sub-satellite joined by a coilable mast obtaining as a result a rigid-flexible multi body system. Flexible vibration of the coilable mast will bring great difficulty and challenge to the control of the micro-satellite.

The first step of this thesis research is to obtain the mathematical model of the rigid-flexible coupling micro-satellite, for this the Lagrange method is used. In terms of dynamics, the coilable mast is normally viewed as a flexible appendage and simplified as an Euler-Bernoulli beam, but the SSS-1 is equipped with a large mass element (sub-satellite) at the tip of the flexible structure, as a consequence and in contrast to previous work, the new mathematical model must include this rigid sub-satellite when deriving the equations of motion.

The satellite is modeled as a body that can rotate in the three axis, the flexible appendage can be affected by lateral deflection while axial and torsional deformation are not considered in this study. Kinetic energy is firstly derived as a natural step in the Lagrange procedure, this consist of the kinetic energy obtained from the three satellite elements (rigid main satellite, flexible coilable mast and rigid sub-satellite). Some matrix notations are used in order to simplified the large total kinetic energy expression and using the assumed modes method the mass matrix of the entire system can be obtained. The stiffness and damping matrices of the model are obtained by defining the potential energy of the system and then applying the assumed modes method for discretization.

In this project large and fast rotations are not considered, therefore lateral deformation of the flexible appendage is not too large. This assumption permits to linearize the obtained dynamic plant to further synthesize a linear controller for direct attitude control and vibration suppression.

Two controllers are proposed to work with the dynamic plant in close loop configuration, the first is the H infinity controller which main purpose is to minimize the impact of the exogenous inputs (w) into the regulated outputs (z). For this the norm of the transfer function known as LFT from w to z must be minimized. The second controller is obtained by using the μ synthesis, in contrast to the first proposed controller this procedure is capable of considering the parametric uncertainty of the system while deriving a robust controller.

Regarding the control strategy, the dynamic plant is interconnected with different weighting functions that can prioritize some task over others. In this project the control system priority is to set the entire structure in the desire orientation, after this the system focuses on suppress the vibration of the flexible appendage. As sensor data the system will the three Euler angles and the lateral acceleration of the displacement of the flexible appendage. Results obtained from the two synthesized controllers are compared when working with the nominal and uncertain dynamic plant.

Keywords: Dynamics, Lagrange, Mechanical Vibrations, Robust Control

Contents

List of Figures

1 Introduction

1.1 Background

Modern days technology allowed many devices to become smaller thorough time, but size was not the only optimized factor, price and efficiency were largely improved too. In the field of astronautics, satellites were known as large and complex devices that were able to perform certain tasks depending on the assigned mission(communications, mapping, global positioning, etc) most of these satellites were huge, heavy and considerably expensive, as a consequence only the most developed and richest countries were capable of designing and manufacture them. As time passed satellites became smaller, cost/efficiency ratio was improved up to the point that terms micro, pico and nano are now used for very small and affordable satellites.

The Attitude Determination and Control system, also known as ADCS, is an essential part in most of satellites where orientation has to be controlled since functionality and fulfillment of mission depends on it, this is the case for very specific applications like remote sensing or spying. Satellite's sensors are in charge of obtaining information about: Angular Velocity (Gyroscopes), Sun Position (Sun-sensor), Magnetic Field (Magnetometer), Infrared Radiation (Earth Horizon sensor) or in some cases galactic reference position (Star-sensor).

Sensor's data is gathered to estimate the satellite's orientation for its correction if needed. Once the satellite's orientation is determined the on-board actuators generate the control torques to rotate the satellite to a desired position . The SSS-1P has three magnetorquers and one reaction wheel that are used for active control of the satellite's attitude. Magnetoquers are coil based actuators that interact with earth's magnetic field to generate a magnetic moment. These are one of the simplest control actuators used on satellites, nevertheless under the relative absence of earth magnetic field the generation of torque is no longer feasible. Reaction wheels on the other hand are not only more precise actuators but also these devices work independently of any magnetic field.

In contrast to other satellites the SSS-1P satellite consist of a rigid main body that deploys a coilable mast that contains at the top a sub-satellite. Due to this the satellite dynamics are not the same as in the case of rigid satellites. The coilable mast must be consider as a flexible structure, due to this the satellite is exposed to bending deformations that generate unexpected

and non parametric disturbances that the attitude control system must suppress.

Deployable structures on space are very common since this characteristic on spacecrafts carry some advantages, one of this is the low launching volume [3]. When launching it is well known that the payload's weight is a very important limiting factor, since not all rockets can carry all kind of payloads, but also payload's volume is just as important since a rocket cannot grow in size to carry all kind of spacecrafts or satellites, instead all payloads must fit inside without consideration.

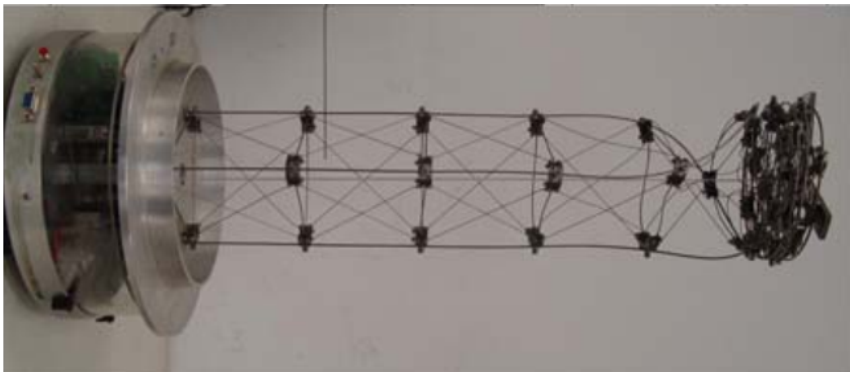

Figure 1: BUAA-sat Coilable mast [1]

Here is where structures with deployable appendages become useful. During launch and before detumbling the satellite can remain rigid as a compact body, once the spacecraft is delivered to its required orbit all deployable components extend until final configuration is obtained. In the case of the SSS-1 its deployable appendage is a flexible coilable mast, similar to the one in figure 1. As can be seen, deployable structures do not only guarantee a practical way of deliver large satellites, but also reduces the weight since many of this structures are lightweight [4] [5].

Even though this kind of advantages are highly desirable this type of structures are also non-rigid. As a consequence flexibility comes with the vibration problem and it cannot be neglected. As can be seen in next figure, flexibility can have an impact on satellite dynamics.

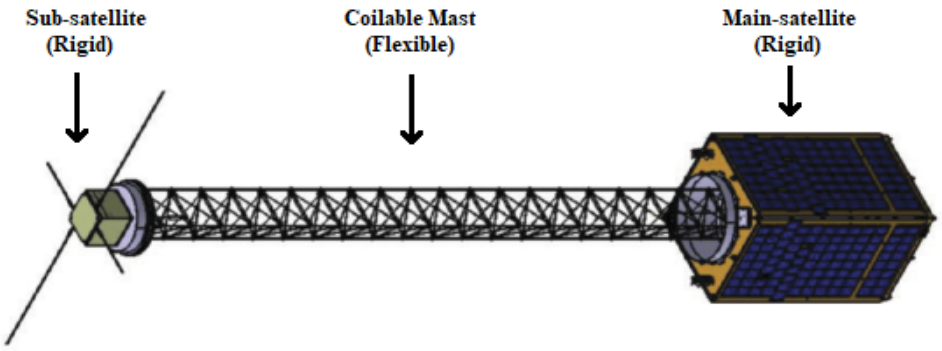

Figure 2: BUAA-sat Coilable mast [2]

As can be seen, for a satellite such as the SSS-1 it is necessary to consider the flexible structure in the dynamics modeling. Also is important to note that the vibration of the flexible appendage affects the entire structure including the main rigid satellite. The two main objectives of this research project are described in the next sub-section.

1.2 Objectives

- **Mathematical model development of the rigid-flexible satellite:**

  An analytical approach based on the Lagrange method is followed in order to obtain the equations of motion. This procedure must include the presence of a body (sub-satellite) at the tip of the flexible appendage. The system dynamics will be time and space dependent due to the presence of a continuous body, so the assumed modes method will be used as discretization technique. Finally parametric uncertainty is inserted in the obtained dynamic plant.

- **Development of a control technique and synthesis of a robust controller:**

  The obtained dynamic plant is linearized and interconnected with weighting function blocks that will specified control priorities of the close loop system. Two different controllers (H_∞ and μ) will be synthesized and compared while working with the nominal and uncertain plant.

1.3 Literature Review

The Attitude Control in contrast to other satellite subsystems has a greater complexity and importance on every mission. The ADCS is in charge of controlling the satellite's orientation during its mission [6, 7], it could be used to steer the satellite on a desired direction or counter the external disturbance forces on it. The AFIT 6u cube-sat explains at [8] the development of the ADCS subsystem based on four reaction wheels that provides redundancy in the case of failure of one actuator or power loss.
The Delfi-n3Xt is the second generation 3U cubesat developed by TuDelft that works with an active attitude control [9]. The Delfi-n3Xt uses a magnetometer and home made photo-diode sun sensors, for 3-axis attitude control three reaction wells and three magnetorquers [10] are used as actuators, the ADCS will work on five different modes: detumbling, coarse sun pointing, fine sun pointing, ground station tracking and experimental thruster pointing.

The ADCS test can be performed by generating a close approximation of space environment by using an air bearing system and a geomagnetic field simulator. MIT Space Systems Laboratory designed and implemented a 4-coild per axis Helmholtz cage with a spherical air bearing for testing attitude determination and control of cube-satellites [11]. Mentioned Helmholtz cage was used as a test bed for the Microsized Microwave Atmospheric Satellite (MicroMAS) ADCS [12], in contrast to previously mentioned satellites the MicroMAS uses an Earth Horizon static Sensor (EHS) that was designed specifically for nano-satellites [13, 14]. All previously mentioned literature assumes the satellite as a rigid body, therefore its dynamic model and control are designed from this structural premise. In the case of a satellite such as the SSS-1P a coilable mast is extended, this appendage is flexible therefore it generates bending moments due to external disturbance sources or control torques from main rigid satellite which contains the ADCS actuators.

It must remain, the dynamics of a flexible structure are not as simple as the dynamics of a rigid body, as a consequence new approaches for deriving the equations of motion must be taken into consideration. Like most of current research on the topic, a flexible structure or appendage such as solar panels or a extendable booms are considered as flexible beams.

In [15] the dynamics and control of a rotating Euler-Bernoulli beam are derived by considering not only the transverse deformation, but also the axial deformation which is a consequence of the beam's centrifugal force, nevertheless, after deriving the equations of motion by using the extended Hamilton's principle the axial deformation was neglected to preserve simpleness. This system simplification is observed in most of research on this topic [16–19] since impact of axial deformation is not considerable nor as important as transverse deformation as long as the angular speeds are below to the first natural frequency [20].

In other cases the flexible appendage has a payload located at the tip, this will also affect the satellite dynamics. In [21] the impact of a mass at the end of a rotating beam is analyzed in detail and the impact of the centrifugal force on the potential energy is derived so it can be considered to create a more accurate dynamic model of the system by using Lagrange or Hamiltonian approach. Like in previous cases, the axial deformation (generated by the centrifugal force) is neglected and only the kinetic energy generated by the payload at appendage tip is considered [22–27].

According to [28] the presence of structures such as solar panels, booms, antennae and their constant increase in size plays an important role in pointing accuracy requirements, modeling and understanding of flexibility is crucial for attitude control problem. In the case of flexible satellites the assumption of a rotating beam with a mass or payload at the tip is widely used due to the fact that most of appendages can be view as rotating beams. In [29, 30] the dynamics of a satellite with one deployable solar panel are modeled while the kinetic and potential energy are obtained from the central hub and a flexible beam attached together, then non linearities are neglected and a vibration suppression control technique is designed. The case of a satellite with two deployable solar panels is analyzed in [31] where structural damping is taken as a non conservative force and the impact of the kinetic and potential energy is duplicated in contrast to previous cases with only one flexible element.

In [32] the author proposes a composite controller with a hierarchical architecture by combing a disturbance-observer-based control (DOBC) and proportional derivative PD control. The problem, which includes only one rigid body and one flexible appendage, is simplified to only one axis of rotation. In this case the DOBC controller is considered to be a robust control scheme where the modeling error can be estimated and compensated [33].

In [30] it is stated that linearization of the satellite's model carry a lost of important information related to the true dynamics of the satellite. Therefore, parametric and non parametric uncertainties from the system must be included, an H_∞ control technique is used combined with the uncertainty model so a more robust and reliable controller can be obtained

According to [34] the problem of attitude determination and control for flexible spacecraft is linked not only to the parametric uncertainties but also to time-varying parameters and imprecise collocation of attitude determination sensors. Since many factors are not included after the linearization of the satellite's dynamics a robust controller is required. This paper proposes an integrated H_∞, including an output feedback and a feed-forward component.

One of the most common flexible satellite problems is related to the Honey Comb type solar panels used by many types of satellites, this type of structure are largely preferred due to its light mass that reduces considerably the spacecraft's weight. At [35] a proportional-derivative controller integrated with the input shaping technique is proposed as a control method for attitude maneuver and vibration suppression. The equations of motion and the boundary conditions are derived by using the Hamiltonian Principle.

A rigid body attached to flexible appendages is also analyzed at [36] by using an adaptive control system for orbiting satellite with described characteristics. The control method used is the $\mathcal{L}_1$ developed by Havokimyan and Cao in [37]. The control system includes a state predictor for unknown parameters generation and it is only studied for the pitch angle and its correspondent derivative. Like all previously mentioned control methods the $\mathcal{L}_1$ is also suitable for parametric uncertainties generated not only by vibration of flexible structures but also for unexpected disturbances.

In [38] two control laws are implemented to guarantee convergence of the closed loop system without using any angular velocity measurement. This quaternion based method describes a partial state feedback where the modal variables describing flexible elements are not measurable. Implemented controller has two features, one is in the form of an observer-based feedback and another where the angular velocity feedback is not used [39] [40].

1.4 Report's Content

This final thesis report is divided in six chapters, each develop important aspects of the thesis research project. The first introductory chapter contains relevant background related to the topics of small satellites, attitude determination and control (ADCS) and its applications. A brief explanation about flexible structures and satellites is also included in this section.

This first chapter also contains a literature survey where previous research and work on attitude determination and control of small satellites is addressed. Different types of small satellites are defined while its characteristics related to the ADCs system and testing are explained, most of this small satellites are modeled as rigid bodies in contrast to the objective of this thesis research project. The second part of the literature review contains relevant research in the field of flexible structures and dynamics modeling, most of these are assumed as Euler-Bernoulli beams.Last part of the literature review explains the previous research on control techniques of flexible structures. Since most of this dynamics are complex it is important to obtain a controller capable of dealing not only with external disturbances but with also parametric uncertainties.

The second chapter addresses relevant theory background. The first part explains the most commonly used techniques for deriving the equations of motion. Then the chapter follows to define the discretization technique that will be used in the research project. This chapter also gives a brief explanation of the sensitivity function and its importance. Following, the most relevant theory behind the H_∞ and μ synthesis control is also included in section two.

Chapter three addresses the problem of the flexible satellite itself by deriving the equations of motion using the Lagrange method and the assumed modes method for system discretization. The model is finally linearized for further controller synthesis.

Chapter four describes the controller strategy. In this case weighting functions are defined in order to prioritize some controller tasks over the others, sensor data is obtained and controllers H_∞ and μ synthesis are obtained.

On Chapter five the close loop system is tested using the two mentioned controllers. Test was performed in two scenarios, the first only considers the nominal dynamic plant, and the second includes parametric uncertainty. Results are analyzed and effectiveness of both controllers are compared

Finally, chapter six addresses the conclusions driven from the research, some future extensions of this work are also included.

2 Theoretical Background

This section contains the most relevant theory background related to the project's development. First, the fundamental methods to formulate the equations of motion (EOM) for structures conformed of rigid and deformable bodies are reviewed. Second, the discretization method, which allows to analyze the dynamics of a continuous body in a discrete manner and finally the H_∞ control synthesis technique, which minimizes the impact of external disturbances and noise on the system is analyzed.

2.1 Formulating the Equations of Motion

Since the proposed system is composed not only of unique particles but of continuous structures the system dynamics are represented by partial differential equations, since each point of a deformable structure will be in a particular position at a particular time, which means that the system is not longer only time dependent but also space dependent. There are two known way to obtain this differential equations of motion, the Lagrangian approach and the extended Hamilton's principle. Even though the Lagrangian method is the one that will be used on this report the extended Hamilton's principle will be explained just for completeness.

2.1.1 Extended Hamilton's Method

This is the most common variational principle of mechanics and according to [41] it can be view as an integrated form of the d'Alembert's principle. Like the Lagrange method, it uses the variation of kinetic and potential energy and the work done by Non-conservative forces such as the viscous damping and the Rayleigh dissipation function to derive the equations of motion. The generalized Hamilton's principle is given by the variational statement:

$$\int_{t_1}^{t_2} \delta(T - V)dt + \int_{t_1}^{t_2} \delta W_{nc} dt = 0 \tag{1}$$

Where T represents the kinetic energy, V the potential energy, δ is known as the variational operator and δW_{nc} is the virtual work done by non conservative forces. Kinetic energy is expressed in terms of the generalize coordinates and their time derivatives, potential energy only depends on the generalize coordinates and the virtual work done by the non-conservative forces is expressed as a linear function of the virtual displacement:

$$\begin{aligned} T &= T(q_1, q_2, ..., q_N, \dot{q}_1, \dot{q}_2, ..., \dot{q}_N, t) \\ V &= V(q_1, q_2, ..., q_N, t) \\ \delta W_{nc} &= Q_1 \delta q_1 + Q_2 \delta q_2 + ... + Q_N \delta q_N \end{aligned} \tag{2}$$

The generalized forces and the coordinates are represented by Q_i and q_i respectively, N represents the number of independent variables. Even though the concept is considered as straightforward its calculation and the algebra required include integration by parts, which makes the EOM formulation process tedious and it becomes even more complicated while dealing with multi body or hybrid systems. Lagrange approach becomes an alternative.

2.1.2 Lagrange Method

By replacing (2) into (1), taking variations and integrating by parts [41] leads to:

$$\frac{d}{dt}(\frac{\partial \mathscr{L}}{\partial \dot{q}_i}) - \frac{\partial \mathscr{L}}{\partial q_i} = Q_i, \quad i = 1, 2, ...N \tag{3}$$

Which is known as the Lagrange equation, where the Lagrangian $\mathscr{L}$ is defined as:

$$\mathscr{L} = T - V \tag{4}$$

System's damping can be included on the Lagrange formulation by using the Rayleigh dissipation function, which allows to represent the entire set of viscous damping forces as a single scalar:

$$\mathscr{R} = \frac{1}{2} \sum_{i=1}^{n} \sum_{i=1}^{n} c_{ij} \dot{q}_i \dot{q}_j \tag{5}$$

By separating the non-conservative forces on equation (3) on viscous dissipative forces and other external forces such us external control torques, the Lagrange equation can be finally expressed as:

$$\frac{d}{dt}(\frac{\partial \mathscr{L}}{\partial \dot{q}_i}) - \frac{\partial \mathscr{L}}{\partial q_i} + \frac{\partial \mathscr{R}}{\partial \dot{q}_i} = Q_i, \quad i = 1, 2, ...N \tag{6}$$

2.2 Finite-Dimensional Analysis of Continuous System

In contrast to particle-composed or rigid-body systems which variables are only time dependent, a flexible structure system such as the case of a satellite with a flexible appendage must be represented by variables that are time and space dependent. This introduces in the system partial differential equations which not are not only harder to deal with analytically, but also computationally [42] [43]. The two most common methods for spatial discretization are the assumed modes method (the one that will be used in this project) and the finite element method [44].

2.2.1 Assumed Modes Method

As previously mentioned, the derived equations of motion for a continuous system are time and space dependent. The assumed modes method represents the structural deflection $y(x,t)$ by finite series of space dependent functions multiplied by time dependent functions, in other words: the assumed modes method divides the time/space defined deflection into two separated functions, each of them dependent only in time or space:

$$y(x,t) = \sum_{i=1}^{N} \phi_i(x) q_i(t) \tag{7}$$

Where $\phi_i(x)$ represents the i_{th} mode shape, and N denotes the number of degrees of freedom for the discrete approximation. This new deflection representation will be used in conjunction with the Lagrangian method in terms of the generalize coordinates. By using equation (7) the kinetic and potential energy can be represented as:

$$\begin{aligned} T(t) &= \tfrac{1}{2}\textstyle\sum_{i=1}^{N}[M]_{ij}\dot{q}_i\dot{q}_j = \tfrac{1}{2}\dot{q}^T M\dot{q} \\ V(t) &= \tfrac{1}{2}\textstyle\sum_{i=1}^{N}[K]_{ij}q_i q_j = \tfrac{1}{2}q^T Kq \end{aligned} \tag{8}$$

Where M_{ij} and K_{ij} denote the (i,j)th element of the mass matrix M and the stiffness matrix K respectively. The damping matrix C and it elements can be derived from equation (5). Finally the equations of motion are calculated by using the Lagrange equation (6) considering the Lagrangian as $\mathscr{L} = T - V$. With the Lagrangian defined, the equations of motion can be easily derived by replacing the values of (8) into (5):

$$\sum_{j=1}^{N}[M]_{rj}\ddot{q}_j(t) + \sum_{j=1}^{N}[C]_{rj}\dot{q}_j(t) + \sum_{j=1}^{N}[K]_{rj}q_j(t) = Q_r \quad r = 1, ..., N \tag{9}$$

Expressed in compact matrix form:

$$M\ddot{q}(t) + C\dot{q}(t) + Kq(t) = Q(t) \tag{10}$$

Note that the equation of motion at (10) looks very familiar, this is because it is similar to the common dynamic representation of the simple mass-spring-damper system, but the most important thing is that the coordinate q and its first and second time derivatives ($\ddot{q}$, $\dot{q}$) are only time dependent. In order to retrieve the original coordinate $y(x,t)$ equation (7) can be used.

The assumed modes method is quite attractive due to its simpleness and is very useful as long as it is possible to approximate the mode shapes $\phi_i(x)$. This is the reason why it is the chosen method for the modeling of the rigid-flexible satellite. For more complicated structures with irregular geometric shapes the finite element method (FEM) becomes a more feasible path to follow, since it will be not possible to derive or obtain easily the shape modes.

2.3 Controller Synthesis

The famous British statistician George E.P.Box stated once that "All models are wrong, but some are useful". This simple but very important quote has a deep meaning which becomes more obvious while a model is tested on a real world scenario. It is crucial to know that even if a model has been rigorously derived with all possible consideration to approximate better the real physical system it will never be perfect, as a consequence all modeled systems are in a certain way wrong.

However according to [45] during the early 80's the H_∞ norm as a metric of robustness was proposed and since then the robust control synthesis and the minimization problem became one of the main topics of research in control systems which are not perfectly modeled, also known as systems with uncertainty.

2.3.1 Sensitivity Function

The objective of the H_∞ synthesis is to optimize/minimize the impact of external sources such as noise and disturbance by obtaining an optimal controller K. In figure (3) a feedback control system for the nominal plant P can be observed:

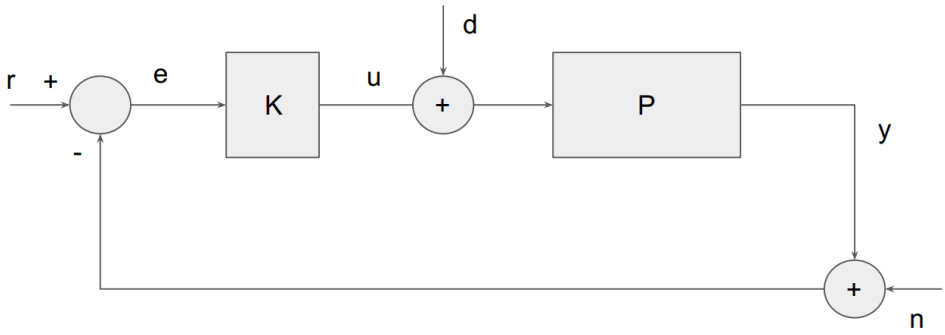

Figure 3: System's Block Diagram

Where r represents a reference signal, u the controller output, d the external disturbances, y is the system's output, n the noise and e is the error between the reference signal and the system's output. System equation is derived:

$$\begin{aligned} y &= P_d d + PK(r - y - n) \\ (I - PK)y &= PKr + P_d d - PKn \end{aligned} \tag{11}$$

By solving equation (11) for y, next equation is obtained

$$y = (I - PK)^{-1}PKr + (I - PK)^{-1}P_d d - (I - PK)^{-1}PKn \tag{12}$$

The term $(I - PK)^{-1}$ is defined as the sensitivity function S, a representation of its magnitude in the frequency domain can be observed in figure 4.

$$S = (I + PK)^{-1} \tag{13}$$

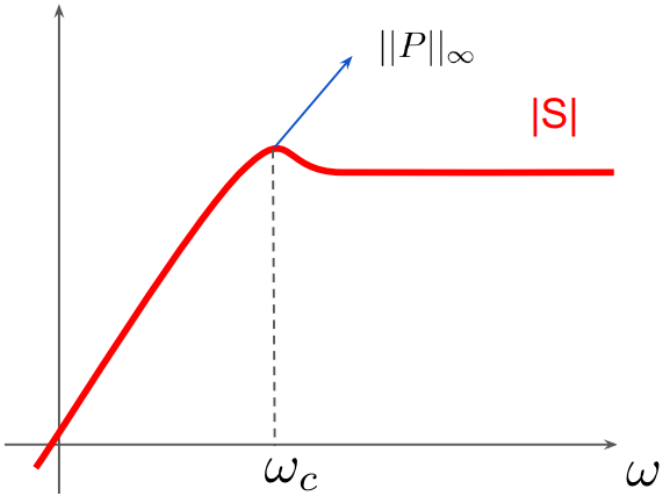

Figure 4: Sensitivity Function in the frequency domain

It can be inferred from equation (13) that as long as the value of $(I - PK)^{-1}$ is small the impact of external elements like noise and disturbances including reference signals (exogenous inputs) will remain small, therefore for having a robust controller that can maintain stability it is important to keep the value of S as small as possible.

2.3.2 H_∞ optimization

It can be seen in figure 4 that the maximum point $||P||_\infty$ of the sensitivity function is located at the cross frequency ω_c. This point represents the H_∞ norm of the plant and like as previously mentioned it must remain small for the system to be robust.

The minimization problem can have different objectives according to the system necessities, a cost function can be derived for each of the following cases [46]:

- For good tracking and disturbance attenuation: $||(I + PK)^{-1}||_\infty$
- For good noise rejection: $|| - (I + Pk)^{-1}PK||_\infty$
- For less control energy: $||K(I + PK)^{-1}||_\infty$

It could be possible for a system to require not only one cost function, such as the case of mixed sensitivity or also known as S over KS problem:

$$\min_{K} \left\| \begin{matrix} (I+PK)^{-1} \\ K(I+PK)^{-1} \end{matrix} \right\| \tag{14}$$

A standard configuration of the system in figure 3 can be obtained by the Linear Fractional Transformation (LFT) technique:

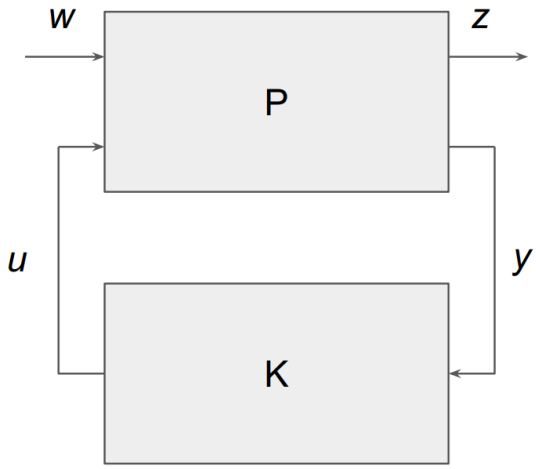

Figure 5: Standard H_∞ configuration

Where w, z, u and y are the exogenous inputs, regulated outputs, controller output and system P output respectively, this plant P is also known as the generalized plant or interconnected system:

$$P(s) = \begin{bmatrix} P_{11}(s) & P_{12}(s) \\ P_{21}(s) & P_{22}(s) \end{bmatrix} \tag{15}$$

This equation is known as the 4-matrix representation and it represents the mapping from the system inputs to its outputs. The minimization problem in this case focuses on reducing the impact of the exogenous inputs w into the regulated outputs z:

$$\begin{aligned} z &= [P_{11} + P_{12}(I - P_{22}K)^{-1}KP_{21}]w \\ z &=: \underline{S}(P,K)w \end{aligned} \tag{16}$$

Where the LFT $\underline{S}(P,K)$ is the lower fractional transformation of P and K. Therefore the H_∞ control problem becomes:

$$\min_K ||S(P,K)|| \tag{17}$$

The generalized plant P can also be defined by its 9-matrix representation:

$$P = \left[\begin{array}{c|cc} A & B_1 & B_2 \\ \hline C_1 & D_{11} & D_{12} \\ C_2 & D_{21} & D_{22} \end{array}\right] \tag{18}$$

Which is the state-space description of the generalize plant P:

$$\begin{aligned} \dot{x}(t) &= Ax(t) + B_1 w(t) + B_2 u(t) \\ z(t) &= C_1 x(t) + D_{11} w(t) + D_{12} u(t) \\ y(t) &= C_2 x(t) + D_{21} w(t) + D_{22} u(t) \end{aligned} \tag{19}$$

Linear Matrix Inequalities (LMIs): As its name states, the linear matrix inequalities are matrix inequalities that are linear in the matrix variables [47], it standard form appears as follows:

$$\begin{gathered} F(X) = x_1 F_1 + x_2 F_2 + ... + x_m F_m \leq F_0 \\ F(x) = \textstyle\sum_{i=1}^{m} x_i F_i - F_0 \leq 0 \end{gathered} \tag{20}$$

Where $x = (x_1, x_2, ..., x_m)$ are unknown scalars called decision variables and $F_i \in \mathbb{R}^{n\times n}$ are known symmetric matrices for $i = 0, ..., m$. The set of solutions $x \in \mathbb{R}^n | F(x) \leq 0$ is assumed as convex, which means that it is possible o formulate a convex optimization problem that minimizes a linear objective function $h(x)$ of a vector of decision variables x with an LMI restrictions as in the form:

$$\min_x h(x) : \Big\{ F(x) \leq 0 \tag{21}$$

The LMI F_x maps a vector space to a cone of semi-defined symmetric matrices.

The Schur Complement Lemma: The Schur complement works as a tool to convert non-linear inequalities (that are non convex) to linear matrix inequalities (LMI). Consider a symmetric matrix P:

$$P = P^T = \begin{bmatrix} A & B \\ B^T & C \end{bmatrix} \tag{22}$$

The Schur complement $\overline{\Delta}_{(.)}$ relative to the inner matrices A and C has the form:

$$\begin{aligned} \overline{\Delta}_A &= C - B^T A^{-1} B \\ \overline{\Delta}_C &= A - B C^{-1} B^T \end{aligned} \tag{23}$$

It can be stated, according to the Schur complement lemma, that:

$$\begin{aligned} P < 0 \iff A < 0, \overline{\Delta}_A < 0 \iff C < 0, \overline{\Delta}_C < 0 \\ P > 0 \iff A > 0, \overline{\Delta}_A > 0 \iff C > 0, \overline{\Delta}_C > 0 \end{aligned} \tag{24}$$

The properties of the Schur complement lemma are used to analyze the positivity of P and to obtain matrix inequalities that define convex regions.

The KYP Lemma: The Kalmam-Popov-Yakubocivh lemma, also known as the Bounded Real Lemma is a widely used theorem in control theory. It can be used to determine the H_∞ norm of a system and for many LMI results [47] [48].
For a system:

$$\begin{aligned} \dot{x}(t) &= Ax(t) + Bu(t) \\ y(t) &= Cx(t) + Du(t) \end{aligned} \tag{25}$$

Where the state matrices A,B,C and D are known and the system can be expressed in matrix form as:

$$\hat{G}(s) = \left[\begin{array}{c|c} A & B \\ \hline C & D \end{array}\right] \tag{26}$$

It can be stated that the following are equivalent:

$$\begin{gathered} 1)\ ||G||_{H_\infty} \leq \gamma \\ 2)\ \text{There exists a X} > 0 \text{ such that:} \\ \begin{bmatrix} A^T X + XA & XB \\ B^T X & -\gamma \end{bmatrix} + \frac{1}{\gamma} \begin{bmatrix} C^T \\ D^T \end{bmatrix} \begin{bmatrix} C & D \end{bmatrix} < 0 \end{gathered} \tag{27}$$

Obtaining a close loop representation for the LFT: Recall the H_∞ standard configuration in figure 5, now the plant P and controller K are defined as:

$$P = \left[\begin{array}{c|cc} A & B_1 & B_2 \\ \hline C_1 & D_{11} & D_{12} \\ C_2 & D_{21} & D_{22} \end{array}\right] \tag{28}$$

$$K = \left[\begin{array}{c|c} A_K & B_K \\ \hline C_K & D_K \end{array}\right] \tag{29}$$

And $\underline{S}(P, K)$ is the LFT that maps the exogenous inputs w to the regulated outputs z. Considering a general case where the controller K is not static and has internal dynamics, the state space representation of the plant and the controller can be written as:

$$\begin{aligned} \dot{x}(t) &= Ax(t) + B_1 w(t) + B_2 u(t) \\ z(t) &= C_1 x(t) + D_{11} w(t) + D_{12} u(t) \\ y(t) &= C_2 x(t) + D_{21} w(t) + D_{22} u(t) \end{aligned} \tag{30}$$

$$\begin{aligned} \dot{x}_K(t) &= A_k x_K(t) + B_K y(t) \\ u(t) &= C_K x_K(t) + D_K y(t) \end{aligned} \tag{31}$$

The objective is to find a close loop state space representation of $\underline{S}(P,K)$. The interconnected system:

$$\begin{bmatrix} \dot{x}(t) \\ \dot{x}_K(t) \end{bmatrix} = \begin{bmatrix} A & 0 \\ 0 & A_K \end{bmatrix} \begin{bmatrix} x(t) \\ x_K(t) \end{bmatrix} + \begin{bmatrix} B_2 & 0 \\ 0 & B_K \end{bmatrix} \begin{bmatrix} u(t) \\ y(t) \end{bmatrix} + \begin{bmatrix} B_1 \\ 0 \end{bmatrix} w(t)$$
$$z(t) = \begin{bmatrix} C_1 & 0 \end{bmatrix} \begin{bmatrix} x(t) \\ x_K(t) \end{bmatrix} + \begin{bmatrix} D_{12} & 0 \end{bmatrix} \begin{bmatrix} u(t) \\ y(t) \end{bmatrix} + D_{11} w(t) \tag{32}$$

From controller and plant output next two equations are obtained:

$$\begin{aligned} u(t) &= D_K y(t) + C_K x_K(t) \\ y(t) &= D_{22} u(t) + C_2 x(t) + D_{21} w(t) \end{aligned} \tag{33}$$

Its matrix representation:

$$\begin{bmatrix} I & -D_K \\ -D_{22} & I \end{bmatrix} \begin{bmatrix} u(t) \\ y(t) \end{bmatrix} = \begin{bmatrix} 0 & C_K \\ C_2 & 0 \end{bmatrix} \begin{bmatrix} x(t) \\ x_K(t) \end{bmatrix} + \begin{bmatrix} 0 \\ D_{21} \end{bmatrix} w(t) \tag{34}$$

The close loop representation can be obtained by replacing equation (34) into equation (32):

$$\begin{bmatrix} \dot{x}(t) \\ \dot{x}_K(t) \end{bmatrix} = A_{CL} \begin{bmatrix} x(t) \\ x_K(t) \end{bmatrix} + B_{CL} w(t)$$
$$z(t) = C_{CL} \begin{bmatrix} x(t) \\ x_K(t) \end{bmatrix} + D_{CL} w(t) \tag{35}$$

Where:

$$A_{CL} = \begin{bmatrix} A & 0 \\ 0 & A_K \end{bmatrix} + \begin{bmatrix} B_2 & 0 \\ 0 & B_K \end{bmatrix} \begin{bmatrix} I & -D_K \\ -D_{22} & I \end{bmatrix}^{-1} \begin{bmatrix} 0 & C_K \\ C_2 & 0 \end{bmatrix}$$
$$B_{CL} = \begin{bmatrix} B_1 + B_2 D_K Q D_{21} \\ B_K Q_{21} \end{bmatrix}$$
$$C_{CL} = \begin{bmatrix} C_1 & 0 \end{bmatrix} + \begin{bmatrix} D_{12} & 0 \end{bmatrix} \begin{bmatrix} I & -D_K \\ -D_{22} & I \end{bmatrix}^{-1} \begin{bmatrix} 0 & C_K \\ C_2 & 0 \end{bmatrix} \tag{36}$$
$$D_{CL} = D_{11} + D_{12} D_K Q D_{21}$$
$$Q = (I - D_{22} D_K)^{-1}$$

The interconnection between the plant and controller trough the LFT $\underline{S}(P,K)$ is well posed if only if the expression at equation (36) is invertible:

$$\begin{bmatrix} I & -D_K \\ -D_{22} & I \end{bmatrix} \tag{37}$$

The inverse of equation (37) is:

$$\begin{bmatrix} I & -D_K \\ -D_{22} & I \end{bmatrix}^{-1} = \begin{bmatrix} I + D_K Q D_{22} & D_K Q \\ Q D_{22} & Q \end{bmatrix} \tag{38}$$

Therefore as long as $Q = (I - D_K D_{22})$ equation at (37) is invertible and the interconnection $\underline{S}(P,K)$ is well-posed, as a consequence a valid close loop expression for the close loop LFT $\underline{S}(P,K)$ was found. Note that if $D_K = 0$ or $D_{22} = 0$ the system interconnection is intrinsically well-posed. It was stated at equations (17) and (18) that H_∞ controller synthesis was based on finding a controller K that could minimize the H_∞ norm of $\underline{S}$(P,K):

$$\min_K ||P_{11} + P_{12}(I - KP_{22})^{-1} K P_{21}||_{H_\infty} \tag{39}$$

Since in previous section a valid state space close loop representation was found at equation (35) it is now possible to say that expression at equation (39) is equivalent to:

$$\min_{\left[\begin{array}{c|c} A_K & B_K \\ \hline C_K & D_K \end{array}\right]} \left|\left| \left[\begin{array}{c|c} A_{CL} & B_{CL} \\ \hline C_{CL} & D_{CL} \end{array}\right] \right|\right|_{H_\infty} \tag{40}$$

Where A_K, B_K, C_K and D_K, refer to the H_∞ controller computed to minimize the H_∞ norm of the close loop system.

2.3.3 Parametric uncertainty and μ synthesis

Parametric uncertainty refers to the inaccurate description of component characteristics. In contrast to a nominal model, which refers to the dynamic modeling without uncertainty on the parameters, an uncertain system present a variation in its characteristics and response to external inputs. The parametric uncertainty modeling problem is concerned with constructing the state-space model [49].

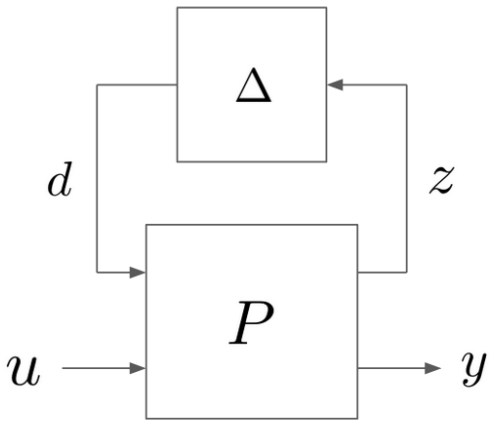

Figure 6: Standard P-Δ configuration

Where Δ represent the perturbation block, it contains all the uncertainties of each parameter $[\delta_1 \ \ \delta_2 \ \ ... \ \ \delta_n]$ in diagonal form

$$\Delta = \begin{bmatrix} \delta_1 & 0 & ... & 0 \\ 0 & \delta_2 & ... & 0 \\ ... & ... & ... & 0 \\ 0 & ... & 0 & \delta_n \end{bmatrix} \tag{41}$$

In some cases a controller obtained through H_∞ synthesis will not be capable of dealing with large parametric uncertainties, creating a not optimal solution or a unstable close loop plant. Another control technique that considers the parametric uncertainty block Δ is the μ synthesis with DK iteration. μ is as non-negative function that gives a generalization of the value $\bar{\sigma}$ that is useful for analyzing robust stability and performance conditions, it is defined as:

$$\mu(P) = \frac{1}{min\{k_m | det(I - k_m P\Delta) = 0 for structured \Delta, \sigma(\Delta) \leq 1} \tag{42}$$

The μ DK iteration follows the next algorithm:

1. K-step: synthesize an H_∞ controller for the scaled problem $min_k||DN(K)D^{-1}||_\infty$ with a fixed $D(s)$, usually D=I.

2. D-step: Find D(jω) to minimize at each frequency $\bar{\sigma}(DND^{-1}(j\omega))$ with fixed N.

3. Fit the magnitude for each $D(k\omega)$ to a stable and minimum-phase $D(s)$, go to step 1 and repeat until the prespecified convergence tolerance is achieved or the maximun iteration number is reached.

In most of cases the μ synthesis with DK iteration works well, but very important drawback is that the order of the obtained controller can be large. This could be an issue at the moment of implementing the close loop plant on a digital system. As a consequence, order reduction may be needed.

3 Dynamics modeling

3.1 Deriving the equations of motion

In this section the mathematical model of the rigid-flexible satellite will be addressed. The system is composed of a rigid structure (main-satellite), a flexible appendage (coilable mast) and a rigid sub-satellite at the tip. The dynamics of the system will be obtained by using the Lagrange method, therefore kinetic and potential energy of each part will be derived. As discretization technique the assumed modes method will be used in combination with the system energies (T, V) to derive the equations of motion. .

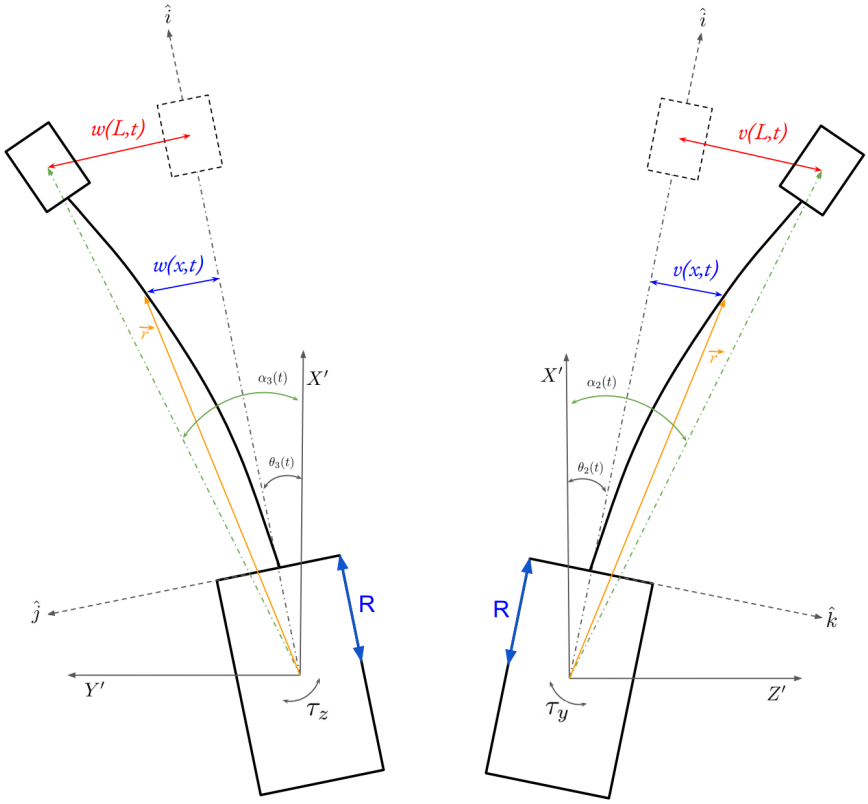

Figure 7: Rigid-flexible satellite representation

From figure 7 it can be observed that the inertial coordinate frame is denoted by the axis X', Y' and Z'. Angular displacement of the thee axis are generated by torques τ_x, τ_y and τ_z. The rigid main satellite has a inertia of J_m, and the distance between its center and the origin of the coilable mast is R. The flexible appendage, assumed as an Euler Bernoulli beam, has a uniform bending stiffness EI, a uniform linear mass density ρ, and a length L.

The rigid sub-satellite at the tip has a mass m and its moment of inertia is J_s. The distance between the center of the main satellite and an arbitrary point at the beam is $\vec{r}$ and the elastic deformations at this specific point is $w(x,t)$ in the $\hat{j}$ direction and $v(x,t)$ in the $\hat{i}$ direction. The elastic deformation at the sub-satellite position depends on $w(L,t)$ and $v(L,t)$, torsional and axial deformation are not considered.

The vector $\vec{r}$ is defined as:

$$\vec{r} = \begin{bmatrix} R+x \\ w(x,t) \\ v(x,t) \end{bmatrix} \tag{43}$$

While its time derivative $\dot{\vec{r}}$:

$$\dot{\vec{r}} = \begin{bmatrix} \dot{\theta}_2 v - \dot{\theta}_3 w \\ -\dot{\theta}_1 v + \dot{\theta}_3 (R+X) + \dot{w} \\ \dot{\theta}_1 w - \dot{\theta}_2 (R+X) + \dot{v} \end{bmatrix} \tag{44}$$

With the $\dot{\vec{r}}$ obtained the satellite kinematics can be derived. Lagrangian approach will be followed in order to obtain the satellite dynamics.

3.1.1 Lagrange Equation

The total kinetic energy T is defined as:

$$T = T_h + T_b + T_s \tag{45}$$

Where T_h, T_b and T_s are the kinetic energy of the main satellite, the flexible beam and the sub-satellite respectively.

$$\begin{aligned} T_h &= \tfrac{1}{2}\dot{\Theta}^T J_h \dot{\Theta} \\ T_b &= \tfrac{1}{2}\rho \int_0^L \dot{\vec{r}}\ \dot{\vec{r}}\ dx \\ T_s &= \tfrac{1}{2} m\ \dot{\vec{r}}_L\ \ \dot{\vec{r}}_L + \tfrac{1}{2}\big[\Theta + ri\big] J_t \big[\Theta + ri\big] \end{aligned} \tag{46}$$

Where:

$$\Theta = \begin{bmatrix}\theta_1 & \theta_2 & \theta_3\end{bmatrix}^T$$

$$ri = \begin{bmatrix}0 & \dot{v}'_L & \dot{w}'_L\end{bmatrix}$$

$$J_h = \begin{bmatrix} J_{h1} & 0 & 0 \\ 0 & J_{h2} & 0 \\ 0 & 0 & J_{h3} \end{bmatrix} \quad J_s = \begin{bmatrix} J_{s1} & 0 & 0 \\ 0 & J_{s2} & 0 \\ 0 & 0 & J_{s3} \end{bmatrix}$$

The expanded kinetic energy of the rigid main satellite:

$$T_h = \tfrac{1}{2} J_{h1} \dot{\theta_1}^2 + \tfrac{1}{2} J_{h2} \dot{\theta_2}^2 + \tfrac{1}{2} J_{h3} \dot{\theta_3}^2 \tag{47}$$

The first time derivative of the position vector $\vec{r}$ is $\dot{\vec{r}}$, its value was defined in equation (44). By replacing the value of $\dot{\vec{r}}$ into T_b at equation (46) the kinetic energy of the beam becomes:

$$\begin{aligned} T_b = \tfrac{1}{2}\rho \int_0^L \left[\dot{\theta}_2 v - \dot{\theta}_3 w\right]^2 dx + \tfrac{1}{2}\rho \int_0^L \left[\dot{\theta}_3 (R+x) + \dot{w} - \dot{\theta}_1 v\right]^2 dx \\ + \tfrac{1}{2}\rho \int_0^L \left[\dot{\theta}_1 w + \dot{v} - \dot{\theta}_2 (R+x)\right]^2 dx \end{aligned} \tag{48}$$

Expanding beam's kinetic energy expression:

$$\begin{aligned} T_b = \tfrac{1}{2}\rho \int_0^L \Big\{ \left[\dot{\theta_2}^2 v^2 - 2\dot{\theta}_2\dot{\theta}_3 v w + \dot{\theta_3}^2 w^2\right] \\ + \left[\dot{\theta_3}^2 (R+x)^2 + 2\dot{\theta}_3 \dot{w}(R+x) - 2\dot{\theta}_3\dot{\theta}_1 v(R+x) + \dot{w}^2 - 2\dot{\theta}_1 \dot{w} v + \dot{\theta_1}^2 v^2\right] \\ + \left[\theta_1^2 w^2 + 2\dot{\theta}_1 w \dot{v} - 2\dot{\theta}_1\dot{\theta}_2 w(R+x) + \dot{v}^2 - 2\dot{v}\dot{\theta}_2(R+x) + \dot{\theta_2}^2 (R+x)^2\right] \Big\} dx \end{aligned} \tag{49}$$

Now the kinetic energy related to the rigid sub-satellite at the tip of the flexible appendage is derived. The first time derivative of the position vector at the tip of the satellite is:

$$\dot{\vec{r}}_L = \begin{bmatrix} \dot{\theta}_2 v_L - \dot{\theta}_3 w_L \\ -\dot{\theta}_1 v_L + \dot{\theta}_3 (R+L) + \dot{w}_L \\ \dot{\theta}_1 w_L - \dot{\theta}_2 (R+L) + \dot{v}_L \end{bmatrix} \tag{50}$$

By replacing this value in equation (46), the kinetic energy of the sub satellite is obtained:

$$\begin{aligned} T_s &= \tfrac{1}{2}m\big[\dot{\theta}_2 v_L - \dot{\theta}_3 w_L\big]^2 + \tfrac{1}{2}m\big[\dot{\theta}_3(R+L) + \dot{w}_L - \dot{\theta}_1 v_L\big]^2 \\ &+\tfrac{1}{2}m\big[\dot{\theta}_1 w_L + \dot{v}_L - \dot{\theta}_2(R+L)\big]^2 + \tfrac{1}{2}\big[J_{s1}\dot{\theta_1}^2 + J_{s2}(\dot{\theta}_2 + \dot{v}'_L)^2 + J_{s3}(\dot{\theta}_3 + \dot{w}'_L)^2\big] \end{aligned} \tag{51}$$

Expanding sub-satellite kinetic energy expression::

$$\begin{aligned} T_s = \tfrac{1}{2}m\big\{&\dot{\theta_3}^2(R+L)^2 + 2\dot{\theta}_3\dot{w}_L(R+L) + \dot{w}_L^2 + \dot{\theta_3}^2 w_L^2 \\ &+\dot{\theta_2}^2(R+L)^2 - 2\dot{\theta_2}\dot{v}_L(R+L) + \dot{v}_L^2 + \dot{\theta_2}^2 v_L^2 + \dot{\theta_1}^2 v_L^2 - 2\dot{\theta_1}\dot{w}_L + \dot{\theta_1}^2 w_L^2 \\ &+2\dot{\theta_1}\dot{v})_L w_L - 2\dot{\theta_2}\dot{\theta_3} v_L w_L - 2\dot{\theta_1}\dot{\theta_2} w_L(R+L) - 2\dot{\theta_3}\dot{\theta_1} v_L(R+L)\big\} \\ &+\tfrac{1}{2}\big\{J_{s1}\dot{\theta_1}^2 + J_{s2}\dot{\theta_2}^2 + 2J_{s2}\dot{\theta_2}\dot{v}'_L + J_{s2}\dot{v}'_L + J_{s3}\dot{\theta_3}^2 + 2J_{s3}\dot{\theta_3}\dot{w}'_L + J_{s3}\dot{w}'^2_L\big\} \end{aligned} \tag{52}$$

The total kinetic energy expression (T) is obtained by replacing results from equations (47), (49) and (52) into (45):

$$\begin{aligned} T = &\tfrac{1}{2}\dot{\theta_3}^2\Big[J_{h3} + \rho\int_0^L (R+x)^2dx + \rho\int_0^L w^2dx + m(R+L)^2 + mw_L^2 + J_{s3}\Big] \\ &+\tfrac{1}{2}\dot{\theta_2}^2\Big[J_{h2} + \rho\int_0^L (R+x)^2dx + \rho\int_0^L v^2dx + m(R+L)^2 + mv_L^2 + J_{s2}\Big] \\ &+\tfrac{1}{2}\dot{\theta_1}^2\Big[J_{h1} + \rho\int_0^L v^2dx + \rho\int_0^L w^2dx + m(w_L)^2 + mv_L^2 + J_{s1}\Big] \\ &+\tfrac{1}{2}\dot{\theta_3}\Big[2\rho\int_0^L (R+x)\dot{w}dx + 2m(R+L)\dot{w}_L + 2J_{s3}\dot{w}'_L\Big] \\ &+\tfrac{1}{2}\dot{\theta_2}\Big[-2\rho\int_0^L (R+x)\dot{v}dx - 2m(R+L)\dot{v}_L + 2J_{s2}\dot{v}'_L\Big] \\ &+\tfrac{1}{2}\dot{\theta_1}\Big[-2\rho\int_0^L v\dot{w}dx - 2mv_L\dot{w}_L + 2\rho\int_0^L w\dot{v}dx + 2mw_L\dot{v}_L\Big] \\ &+\tfrac{1}{2}\Big[\rho\int_0^L \dot{w}^2dx + m\dot{w}_L^2 + J_{s3}\dot{w}'^2_L\Big] + \tfrac{1}{2}\Big[\rho\int_0^L \dot{v}^2dx + m\dot{v}_L^2 + J_{s2}\dot{v}'^2_L\Big] \\ &-\tfrac{1}{2}\Big[2\dot{\theta_2}\dot{\theta_3}\Big(\rho\int_0^L vwdx + mv_Lw_L\Big) + 2\dot{\theta_1}\dot{\theta_2}\Big(\rho\int_0^L w(R+x)dx + mw_L(R+L)\Big) \\ &+2\dot{\theta_3}\dot{\theta_1}\Big(\rho\int_0^L v(R+x)dx + mv_L(R+L)\Big)\Big] \end{aligned} \tag{53}$$

The main issue with this expression is its size. As a consequence, obtaining the mass matrix M from it can become a tedious task, due to this the whole kinetic equation will be simplified by using composed matrix elements. Flexible appendage deformations such as $w(x,t)$ and $v(x,t)$ are embedded in the R_b matrix.

$$R_b = \begin{bmatrix} 0 & v & -w \\ -v & 0 & (R+x) \\ w & -(R+x) & 0 \end{bmatrix} \tag{54}$$

Note that these deformation ($w(x,t)$ and $v(x,t)$) will no longer be fully expressed with its space and time dependence but just by w and v. The sub satellite moment of inertia is represented in two new different matrices (J_s^* and J_s^{**}). In contrast to the original J_s these new matrices only differ in the position of the inertia elements inside them:

$$J_s^* = \begin{bmatrix} J_{s1} & 0 & 0 \\ 0 & 0 & J_{s3} \\ 0 & J_{s2} & 0 \end{bmatrix} \quad J_s^{**} = \begin{bmatrix} J_{s1} & 0 & 0 \\ 0 & J_{s3} & 0 \\ 0 & 0 & J_{s2} \end{bmatrix} \tag{55}$$

By using these new obtained matrix expressions, the angular position vector Θ and a deformation vector $u = [0 \;\; w \;\; v]$ a more compact expression of the total kinetic energy T is obtained:

$$\begin{aligned} T = \tfrac{1}{2}\rho \int_0^L \dot{\Theta}^T R_b^2 \dot{\Theta} dx - \tfrac{1}{2} m \dot{\Theta}^T R_{bL}^2 \dot{\Theta} + \tfrac{1}{2}\big[2\rho \int_0^L \dot{u}^T R_b \dot{\Theta}\big] + \tfrac{1}{2}\big[\dot{u}_L^T R_{bL} \dot{\Theta}\big] \\ + \tfrac{1}{2}\big[2\dot{u}_L^T J_s^* \dot{\Theta}\big] + \tfrac{1}{2}\rho \int_0^L \dot{u}^2 dx + \tfrac{1}{2} m \dot{u}_L^2 + \tfrac{1}{2}\dot{\Theta} J_h \dot{\Theta} + \tfrac{1}{2}\dot{\Theta} J_s \dot{\Theta} + \tfrac{1}{2}\dot{u}_L' J_s^{**} \dot{u}_L' \end{aligned} \tag{56}$$

The previous step before obtaining the mass matrix M is to separate the kinetic energy in two expressions one in term of angular position vector Θ and the other in terms of the deformation vector u:

$$T_{\dot{\Theta}} = -\tfrac{1}{2}\rho\int_0^L(\dot{\Theta}R_b^2\dot{\Theta})dx - \tfrac{1}{2}m\dot{\Theta}R_{bL}^2\dot{\Theta} + \tfrac{1}{2}\big[\rho\int_0^L(\dot{u}^TR_b\dot{\Theta})dx\big] + \tfrac{1}{2}\big[m\dot{u}_L^TR_{bL}\dot{\Theta}\big]$$
$$+\tfrac{1}{2}\big[\dot{u}_L'J_s^*\dot{\Theta}\big] + \tfrac{1}{2}\dot{\Theta}J_h\dot{\Theta} + \tfrac{1}{2}\dot{\Theta}J_s\dot{\Theta}$$
$$T_u = \tfrac{1}{2}\rho\int_0^L\dot{u}^2dx + \tfrac{1}{2}m\dot{u}_L^2 + \tfrac{1}{2}\big[\rho\int_0^L\dot{u}^TR_b\dot{\Theta}dx\big] + \tfrac{1}{2}\big[m\dot{u}_L^TR_{bL}\dot{\Theta}\big] \tag{57}$$
$$+\tfrac{1}{2}\big[\dot{u}_L'^TJ_s^{**}\dot{u}_L'\big] + \tfrac{1}{2}\big[\dot{u}_L'^TJ_s^*\dot{\Theta}\big]$$

These two last equation represent the kinetic energy of the rigid-flexible satellite in a more compact way if compared to the original expression at (53). As can be inferred, the flexible appendage is a continuous body, therefor discretization of the flexible system is required. Like mentioned before the assumed modes method will be used.

3.1.2 Spatial Discretization

As spatial discretization technique the Assumed Modes method, or most commonly known as modal analysis, is used [41]. The assumed mode method allows to represent the time and space dependent function such as $w(x,t)$ as a multiplication of the assumed mode shape $\phi_i(x)$ and the generalize coordinates $q_i(t)$ which are only-space and only-time dependent respectively:

$$w(x,t) = \sum_{i=1}^{N}\phi_i(x)\eta_i(t) \tag{58}$$

Where N defines the number of degrees of freedom. The mode shapes can be found by:

$$\phi_i(x) = C_1(cosh(\beta_i x) - cos(\beta_i x) - K_r(sinh(\beta_i x) - sin(\beta_i x)))$$
$$K_r = \tfrac{cosh(\beta_i L)+cos(\beta_i L)}{sinh(\beta_i L))+sin(\beta_i L)} \tag{59}$$

The values of β_i can be obtained from the transcendental equation, also known as the characteristic equation:

$$1 + cosh(\beta_i L)cos(\beta_i L) + \frac{m}{\rho L}\Big(sinh(\beta_i L)cos(\beta_i L) - cosh(\beta_i L)sin(\beta_i L)\Big) = 0 \tag{60}$$

Assuming that the mass of the sub-satellite is $m = 1\ Kg$, line density of the coilable mast $\rho = 1.5\ Kg/m$, its length $L = 2\ m$ and the number of degrees of freedom $N = 2$. The roots of the transcendental equation can be observed in figure 8.

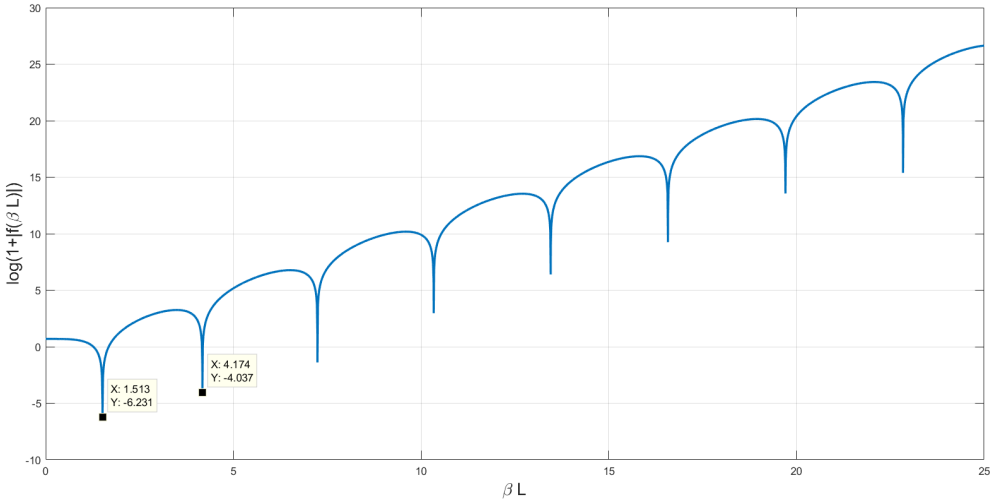

Figure 8: Roots of transcendental equation

Only the first two roots are necessary, since a two degrees of freedom mode is used:

$$\beta_1 = 1.514$$
$$\beta_2 = 4.175$$

The mode shapes then can be obtained by replacing the values of β_1 and β_2 into equation (60). If assuming $\phi = \begin{bmatrix}\phi_1(x) & \phi_2(x)\end{bmatrix}^T$ and $q = \begin{bmatrix}\eta_1 & \eta_2\end{bmatrix}$ a new vector expression for the elastic deformation and velocity at equation (58) is obtained:

$$\begin{aligned} w(x,t) &= \phi_y^T q_y \\ \dot{w}(x,t) &= \phi_y^T \dot{q}_y \\ v(x,t) &= \phi_z^T q_z \\ \dot{v}(x,t) &= \phi_z^T \dot{q}_z \end{aligned} \tag{61}$$

In order to keep the matrix form that allowed to simplify the original T expression the shape modes are now represented as:

$$\Phi = \begin{bmatrix} 0 & 0 & 0 \\ 0 & \phi_1 & 0 \\ 0 & 0 & \phi_2 \end{bmatrix} \tag{62}$$

By applying the assumed modes method for discretization of the kinetic energy, a new simplified T expression is obtained:

$$\begin{gathered} T = \dot{\Theta}^T M_{11} \dot{\Theta} + \dot{q}^T M_{12} \dot{\Theta} \\ \dot{q}^T M_{21} \dot{\Theta} + \dot{q}^T M_{22} \dot{q} \end{gathered} \tag{63}$$

Where:

$$\begin{gathered} M_{11} = -\tfrac{1}{2}\rho \int_0^L R_b^2 dx - \tfrac{1}{2} R_{bL}^2 + \tfrac{1}{2} J_h + \tfrac{1}{2} J_s \\ M_{12} = \tfrac{1}{2}\rho \int_0^L \Phi R_b dx + \tfrac{1}{2} m \Phi_L R_{bL} + \tfrac{1}{2} \Phi_L^{'} J_s^* \\ M_{21} = M_{12}^{'} \\ M_{22} = \tfrac{1}{2}\rho \int_0^L \Phi \Phi dx + \tfrac{1}{2} m \Phi_L \Phi_L + \tfrac{1}{2} \Phi_L^{'} J_s^{**} \Phi_L^{'} \end{gathered} \tag{64}$$

Kinetic energy can be now re-expressed in a matrix form:

$$T = \begin{bmatrix} \dot{\Theta}^T & \dot{q}^T \end{bmatrix} \begin{bmatrix} M_{11} & M_{12} \\ M_{21} & M_{22} \end{bmatrix} \begin{bmatrix} \dot{\Theta} \\ \dot{q} \end{bmatrix} \tag{65}$$

The mass matrix, which is originally denoted as the letter M, is composed of four elements, each of those are derived and calculated in detail:

$$
\begin{aligned}
M_{11} &= \tfrac{1}{2}\begin{bmatrix} J_{hx} & 0 & 0 \\ 0 & J_{hy} & 0 \\ 0 & 0 & J_{hz} \end{bmatrix} + \tfrac{1}{2}\begin{bmatrix} J_{hx} & 0 & 0 \\ 0 & J_{hy} & 0 \\ 0 & 0 & J_{hz} \end{bmatrix} \\
&+\tfrac{1}{2}\rho \int_0^L \begin{bmatrix} -q_1\phi_1^T\phi_1 q_1^T - q_2\phi_2^T\phi_2 q_2^T & q_1(R+x)\phi_1^T & q_2(R+x)\phi_2^T \\ q_1(R+x)\phi_1^T & -(R+x)^2 - q_2\phi_2^T\phi_2 q_2^T & q_2\phi_2^T\phi_1 q_1^T \\ q_2(R+x)\phi_2^T & q_2\phi_2^T\phi_1 q_1^T & -(R+x)^2 - q_1\phi_1^T\phi_1 q_1 \end{bmatrix} dx \\
&+\tfrac{1}{2}m \begin{bmatrix} -q_1\phi_{1L}^T\phi_{1L}q_1^T - q_2\phi_{2L}^T\phi_{2L}q_2^T & q_1(R+L)\phi_{1L}^T & q_2(R+L)\phi_{2L}^T \\ q_1(R+L)\phi_{1L}^T & -(R+L)^2 - q_2\phi_{2L}^T\phi_{2L}q_2^T & q_2\phi_{2L}^T\phi_{1L}q_1^T \\ q_2(R+L)\phi_{2L}^T & q_2\phi_{2L}^T\phi_{1L}q_1^T & -(R+L)^2 - q_1\phi_{1L}^T\phi_{1L}q_1 \end{bmatrix}
\end{aligned}
\tag{66}
$$

$$
\begin{aligned}
M_{12} &= \tfrac{1}{2}\begin{bmatrix} 0 & 0 & 0 \\ 0 & 0 & J_{s3}\phi_{1L}^{'} \\ 0 & J_{s2}\phi_{2L}^{'} & 0 \end{bmatrix} + \tfrac{1}{2}\rho \int_0^L \begin{bmatrix} 0 & 0 & 0 \\ -q_2\phi_1\phi_2 & 0 & \phi_1(R+x) \\ q_1\phi_2\phi_1 & -\phi_2(R+x) & 0 \end{bmatrix} dx \\
&+\tfrac{1}{2}m \begin{bmatrix} 0 & 0 & 0 \\ q_2\phi_{1L}^T\phi_{2L} & 0 & \phi_{1L}(R+L) \\ q_1\phi_{2L}^T\phi_{1L} & -\phi_{2L}(R+L) & 0 \end{bmatrix}
\end{aligned}
\tag{67}
$$

$$
\begin{aligned}
M_{22} &= \tfrac{1}{2}\begin{bmatrix} 0 & 0 & 0 \\ 0 & J_{s3}\phi_{1L}^{'2} & 0 \\ 0 & 0 & J_{s2}\phi_{2L}^{'2} \end{bmatrix} + \tfrac{1}{2}\rho \int_0^L \begin{bmatrix} 0 & 0 & 0 \\ 0 & \phi_1^T\phi_1 & 0 \\ 0 & 0 & \phi_2^T\phi_2 \end{bmatrix} dx \\
&+\tfrac{1}{2}m \begin{bmatrix} 0 & 0 & 0 \\ 0 & \phi_{1L}^T\phi_{1L} & 0 \\ 0 & 0 & \phi_{2L}^T\phi_{2L} \end{bmatrix}
\end{aligned}
\tag{68}
$$

The mass matrix M contains time dependent elements, in order to synthesize an H_∞ or μ controller it is necessary of linearize the plant. Each of the mass matrix elements are linearized around the equilibrium point $q_1 = q_2 = [0]$:

$$M_{11} = \begin{bmatrix} J_1 & 0 & 0 \\ 0 & J_2 & 0 \\ 0 & 0 & J_3 \end{bmatrix} \tag{69}$$

Where:

$$J_1 = J_{h1} + J_{s1}$$

$$J_2 = J_{h2} + J_{s2} + \rho \int_0^L (R+x)^2 dx + m(R+L)^2$$

$$J_3 = J_{h3} + J_{s3} + \rho \int_0^L (R+x)^2 dx + \tfrac{1}{2} m(R+L)^2$$

$$M_{12} = \begin{bmatrix} 0 & 0 & 0 \\ 0 & 0 & M_{rf1} \\ 0 & M_{rf2} & 0 \end{bmatrix} \tag{70}$$

Where:

$$M_{mrf1} = \rho \int_0^L \phi_1 (R+x) dx + m\phi_{1L}(R+L) + J_{s3}\phi'_{1L}$$

$$M_{mrf2} = \rho \int_0^L \phi_2 (R+x) dx + m\phi_{2L}(R+L) + J_{s2}\phi'_{2L}$$

$$M_{22} = \begin{bmatrix} 0 & 0 & 0 \\ 0 & M_{ff1} & 0 \\ 0 & 0 & M_{ff2} \end{bmatrix} \tag{71}$$

Where:

$$M_{ff1} = \int_0^L \phi_1^T \phi_1 dx + \phi_{1L}^T \phi_{1L} + \phi_{1L}'^T \phi'_{1L}$$

$$M_{ff2} = \int_0^L \phi_2^T \phi_2 dx + \phi_{2L}^T \phi_{2L} + \phi_{2L}'^T \phi'_{2L}$$

By replacing equations 69, 70 and 71 in equation 65 the linearize M matrix is obtained:

$$M = \left[\begin{array}{ccc|cc} J_1 & 0 & 0 & 0 & 0 \\ 0 & J_2 & 0 & 0 & M_{rf1} \\ 0 & 0 & J_3 & M_{rf2} & 0 \\ \hline 0 & 0 & M_{rf2}^T & M_{ff1} & 0 \\ 0 & M_{rf1}^T & 0 & 0 & M_{ff2} \end{array}\right] \quad q = \begin{bmatrix} \dot{\theta_1} \\ \dot{\theta_2} \\ \dot{\theta_3} \\ \dot{q_1} \\ \dot{q_2} \end{bmatrix} \tag{72}$$

Total kinetic energy can be expressed as:

$$T = \tfrac{1}{2}\dot{q}[M]\dot{q} \tag{73}$$

The potential energy of the system is calculated in order to obtain the stiffness matrix:

$$V = \frac{1}{2}EI_w \int_0^L w''^2 dx + \frac{1}{2}EI_v \int_0^L v''^2 dx \tag{74}$$

By applying the assumed modes method for discretization, the potential energy becomes:

$$V = \frac{1}{2}EI_w q_1^T \Big(\int_0^L \phi_1''^T \phi_1'' dx \Big) q_1 + \frac{1}{2}EI_v q_2^T \Big(\int_0^L \phi_2''^T \phi_2'' dx \Big) q_2 \tag{75}$$

Stiffness matrix K is can be defined as:

$$K = \begin{bmatrix} 0 & 0 & 0 & 0 & 0 \\ 0 & 0 & 0 & 0 & 0 \\ 0 & 0 & 0 & 0 & 0 \\ 0 & 0 & 0 & K_{ff1} & 0 \\ 0 & 0 & 0 & 0 & K_{ff2} \end{bmatrix} \tag{76}$$

Where:

$$\begin{aligned} K_{ff1} &= EI_w \int_0^L \phi_1''^T \phi_1'' dx \\ K_{ff2} &= EI_v \int_0^L \phi_2''^T \phi_2'' dx \end{aligned} \tag{77}$$

Potential energy can be now expressed as:

$$V = \tfrac{1}{2} q[K]q \tag{78}$$

Damping coefficient is defined as K_e, with it the Rayleigh dissipation function can be obtained:

$$\mathscr{R} = \tfrac{1}{2} \dot{q}[D]\dot{q} \tag{79}$$

The damping matrix of the system is defined as:

$$D = \frac{1}{2} K_{ew} EI_w q_1^T \Big(\int_0^L \phi_1''^T \phi_1'' dx \Big) q_1 + \frac{1}{2} K_{ev} EI_v q_2^T \Big(\int_0^L \phi_2''^T \phi_2'' dx \Big) q_2 \tag{80}$$

In order to derive the system dynamics the first step is to obtain the Lagrangian, defined at equation (4).

$$\mathscr{L} = \frac{1}{2} \dot{q}[M]\dot{q} - \frac{1}{2} q[K]q \tag{81}$$

The second step is to obtain the Lagrange equation defined at (6):

$$\begin{aligned} \tfrac{d}{dt}\big(\tfrac{\partial \mathscr{L}}{\partial \dot{q}}\big) - \tfrac{\partial \mathscr{L}}{\partial q} + \tfrac{\partial \mathscr{R}}{\partial \dot{q}} &= Q \\ \tfrac{d}{dt}([M]\dot{q}) + [K]q + [C]\dot{q} &= Q \end{aligned} \tag{82}$$

Finally the linearize rigid-flexible satellite equation of motion is:

$$[M]\ddot{q} + [K]q + [C]\dot{q} = Q \tag{83}$$

Where the generalize coordinates are defined as $Q = [\tau_x \quad \tau_y \quad \tau_z \quad 0 \quad 0 \quad 0 \quad 0]^T$. The mass, stiffness and damping matrix are numerically calculated by using the system parameters in next section.

3.2 Uncertain Plant

In previous section the equations of the rigid-flexible micro-satellite were obtained, also a linear expression was obtained at equation (83) an it would be used to obtain a state space representation of the system. Nominal values of the system parameter are defined in table 1:

Table 1: Rigid-Flexible satellite parameters

Parameters	**Values**
Length of the beam	L = 2 m
Main satellite radius	R = 0.5 m
Inertia of main satellite	Jm = diag([0.7,2.5,1.5]) $Kg.m^2$
Inertia of sub-satellite	Js = diag([0.4,0.2,0.2]) $Kg.m^2$
Mass of sub satellite	m = 1 Kg
Flexural rigidity of the beam	EI_w = 1.5 EI_v = 1.72 Nm^2
Line density of beam	ρ = 1.5 Kg/m
Damping coefficient	Ke = 0.086

Based on [27] in this project five parameters will be assumed as uncertain:

- Mass of the sub-satellite (m), 15% of uncertainty
- Line density of the beam ($m\rho$), 15% of uncertainty
- Inertia of main-satellite (J_s), 20% of uncertainty
- Inertia of sub-satellite (J_s), 20% of uncertainty
- Flexural rigidity of the beam (EI), 80% of uncertainty

The nominal mass, stiffness and damping matrices are:

$$M = \begin{bmatrix} 0.5500 & 0 & 0 & 0 & 0 & 0 & 0 \\ 0 & 8.3500 & 0 & 0 & 0 & 1.8622 & 0.1894 \\ 0 & 0 & 7.8500 & -1.7518 & -0.6059 & 0 & 0 \\ 0 & 0 & -1.7518 & 0.5304 & -0.1156 & 0 & 0 \\ 0 & 0 & -0.6059 & -0.1156 & 0.9337 & 0 & 0 \\ 0 & 1.8622 & 0 & 0 & 0 & 0.5304 & -0.1156 \\ 0 & 0.1894 & 0 & 0 & 0 & -0.1156 & 0.9337 \end{bmatrix}$$

$$K = \begin{bmatrix} 0 & 0 & 0 & 0 & 0 & 0 & 0 \\ 0 & 0 & 0 & 0 & 0 & 0 & 0 \\ 0 & 0 & 0 & 0 & 0 & 0 & 0 \\ 0 & 0 & 0 & 0.1639 & -0.0001 & 0 & 0 \\ 0 & 0 & 0 & -0.0001 & 9.4872 & 0 & 0 \\ 0 & 0 & 0 & 0 & 0 & 0.1880 & -0.0001 \\ 0 & 0 & 0 & 0 & 0 & -0.0001 & 10.8787 \end{bmatrix}$$

$$D = \begin{bmatrix} 0 & 0 & 0 & 0 & 0 & 0 & 0 \\ 0 & 0 & 0 & 0 & 0 & 0 & 0 \\ 0 & 0 & 0 & 0 & 0 & 0 & 0 \\ 0 & 0 & 0 & 0.0141 & 0 & 0 & 0 \\ 0 & 0 & 0 & 0 & 0.8159 & 0 & 0 \\ 0 & 0 & 0 & 0 & 0 & 0.0162 & 0 \\ 0 & 0 & 0 & 0 & 0 & 0 & 0.9356 \end{bmatrix}$$

The obtained equation of motion of the rigid-flexible satellite at (83) can be represented as a block diagram as shown in figure 9:

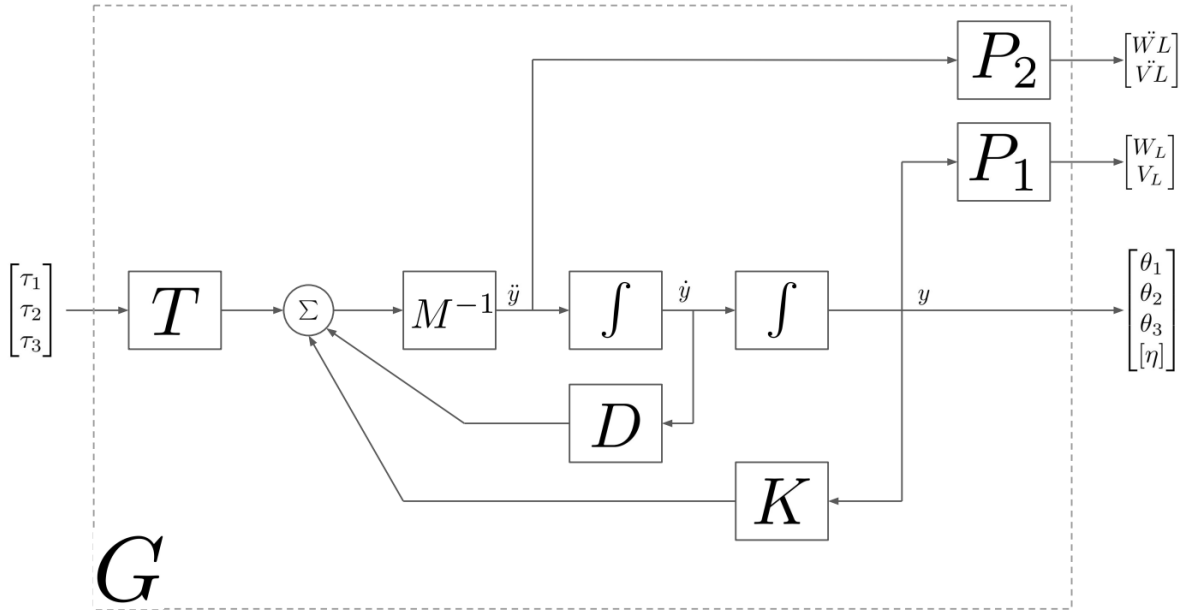

Figure 9: Block diagram of Rigid-Flexible satellite system

The two new blocks P_1 and P_2 are used to obtain the acceleration and displacement at the tip of the flexible appendage ($x = L$):

$$P1 = P2 = \begin{bmatrix} \phi_{1y}(L) & \phi_{2y}(L) \\ \phi_{1z}(L) & \phi_{2z}(L) \end{bmatrix} \tag{84}$$

The obtained nominal state space representation of the interconnected plant G becomes:

$$A = \begin{bmatrix} 0 & 0 & 0 & 0.04 & 0.43 & 0 & 0 & 0 & 0 & 0 & 0.48 & 5.01 \\ 0 & -0.05 & -0.90 & 0 & 0 & 0 & 0 & 0 & -0.59 & -10.41 & 0 & 0 \\ 0 & -0.20 & -3.37 & 0 & 0 & 0 & 0 & 0 & -2.39 & -39.14 & 0 & 0 \\ 0 & -0.06 & -1.87 & 0 & 0 & 0 & 0 & 0 & -0.68 & -21.77 & 0 & 0 \\ 0 & 0 & 0 & -0.18 & -1.78 & 0 & 0 & 0 & 0 & 0 & -2.13 & -20.92 \\ 0 & 0 & 0 & -0.03 & -1.31 & 0 & 0 & 0 & 0 & 0 & -0.361 & -15.26 \\ 0 & 0 & 0 & 0 & 0 & 0 & 0 & 0 & 0 & 0 & 0 & 0 \\ 0 & 0 & 0 & 0 & 0 & 0 & 0 & 0 & 0 & 0 & 0 & 0 \\ 1 & 0 & 0 & 0 & 0 & 0 & 0 & 0 & 0 & 0 & 0 & 0 \\ 0 & 1 & 0 & 0 & 0 & 0 & 0 & 0 & 0 & 0 & 0 & 0 \\ 0 & 0 & 1 & 0 & 0 & 0 & 0 & 0 & 0 & 0 & 0 & 0 \\ 0 & 0 & 0 & 1 & 0 & 0 & 0 & 0 & 0 & 0 & 0 & 0 \\ 0 & 0 & 0 & 0 & 1 & 0 & 0 & 0 & 0 & 0 & 0 & 0 \end{bmatrix}$$

$$B = \begin{bmatrix} 1.8181 & 0 & 0 \\ 0 & 0.70 & 0 \\ 0 & 0 & 1.01 \\ 0 & 0 & 3.57 \\ 0 & 0 & 1.10 \\ 0 & -2.57 & 0 \\ 0 & -0.46 & 0 \\ 0 & 0 & 0 \\ 0 & 0 & 0 \\ 0 & 0 & 0 \\ 0 & 0 & 0 \\ 0 & 0 & 0 \\ 0 & 0 & 0 \\ 0 & 0 & 0 \end{bmatrix}$$

$$C = \begin{bmatrix} 0 & 0 & 0 & 0 & 0 & 0 & 1 & 0 & 0 & 0 & 0 & 0 & 0 \\ 0 & 0 & 0 & 0 & 0 & 0 & 0 & 0 & 1 & 0 & 0 & 0 & 0 \\ 0 & 0 & 0 & 0 & 0 & 0 & 0 & 0 & 0 & 0.76 & -0.404 & 0 & 0 \\ 0 & 0 & -0.13 & -1.81 & 0 & 0 & 0 & 0 & 0 & -1.55 & -21.02 & 0 & 0 \\ 0 & 0 & 0 & 0 & 0 & 0 & 0 & 1 & 0 & 0 & 0 & 0 & 0 \\ 0 & 0 & 0 & 0 & 0 & 0 & 0 & 0 & 0 & 0 & 0 & 0.76 & -0.41 \\ 0 & 0 & 0 & 0 & -0.13 & -0.84 & 0 & 0 & 0 & 0 & 0 & -1.47 & -9.77 \end{bmatrix}$$

$$D = \begin{bmatrix} 0 & 0 & 0 & 0 & 0 & 0 & 0 \\ 0 & 0 & 0 & 0 & 0 & 0 & -1.77 \\ 0 & 0 & 0 & 2.28 & 0 & 0 & 0 \end{bmatrix}^T$$

The bode plots of the rigid flexible satellite system with the driving torque vector $\tau = [\tau_x \quad \tau_y \quad \tau_z]$ as input and $[\theta_1 \ \theta_2 \ \theta_3 \ V_L \ \ddot{V}_L \ W_L \ \ddot{W}_L]$ as outputs are shown in figures 10-16. The frequency response of the nominal system is highlighted in red color, while frequency response of the system with uncertainty correspond to the blue dashed lines.

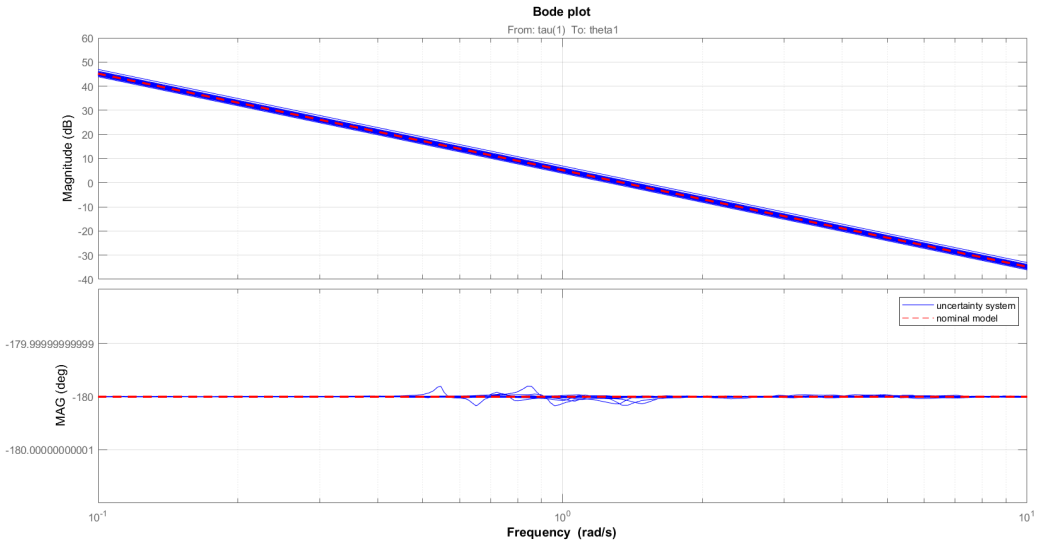

Figure 10: Bode plot from τ_1 to θ_1

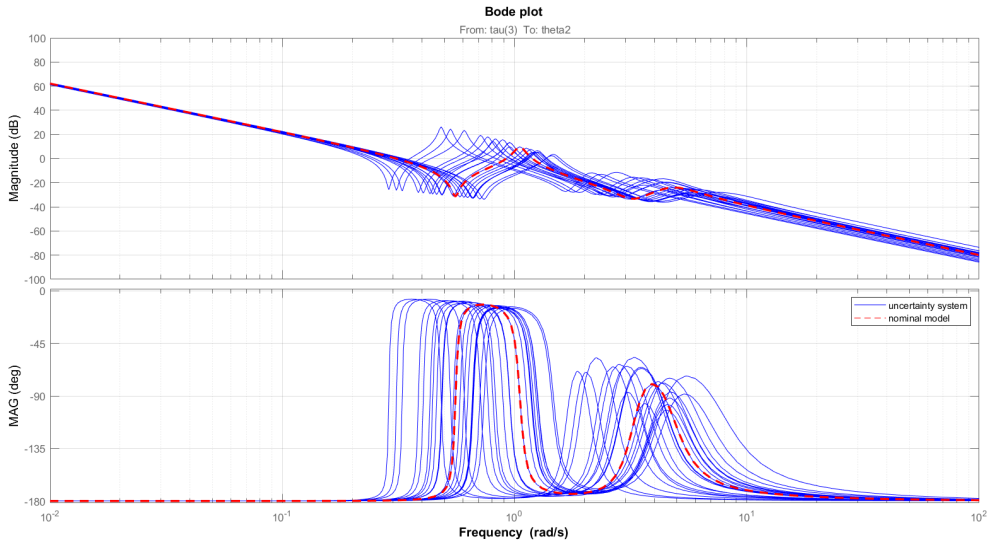

Figure 11: Bode plot from τ_3 to θ_2

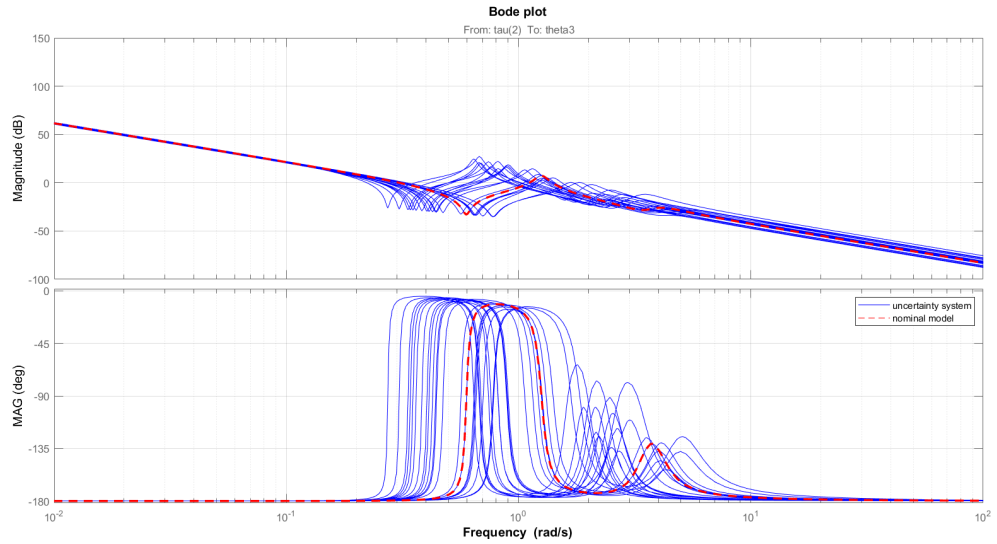

Figure 12: Bode plot from τ_2 to θ_3

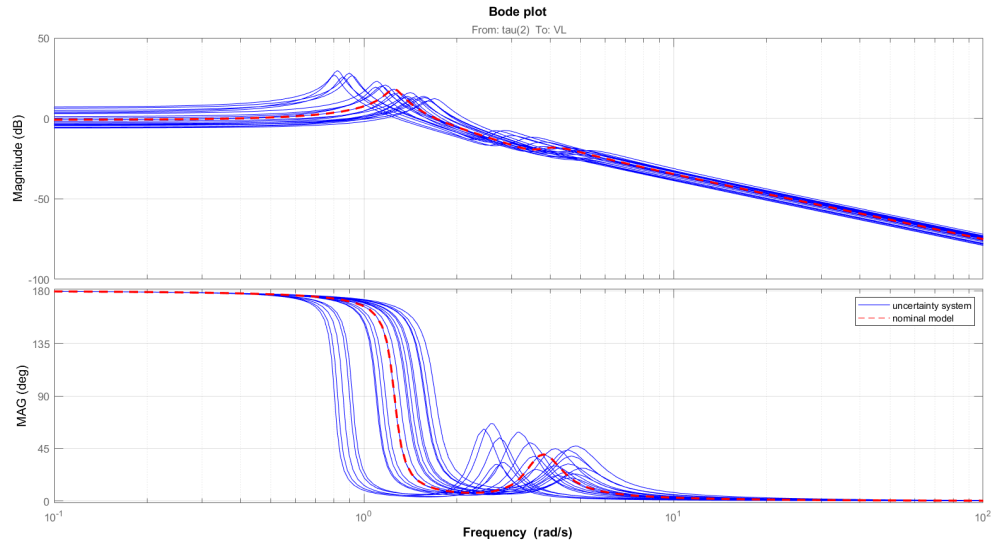

Figure 13: Bode plot from τ_2 to V_L

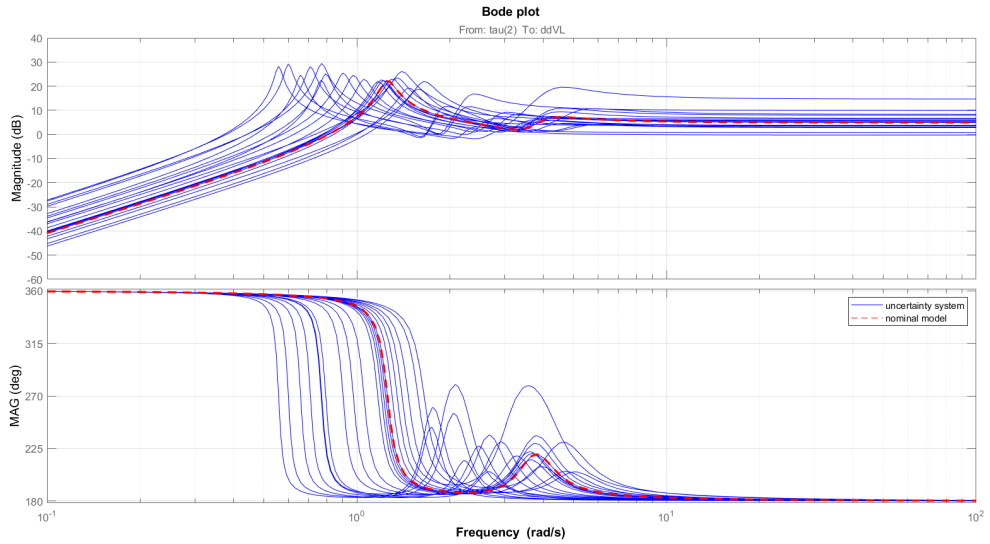

Figure 14: Bode plot from τ_2 to $\ddot{V}_L$

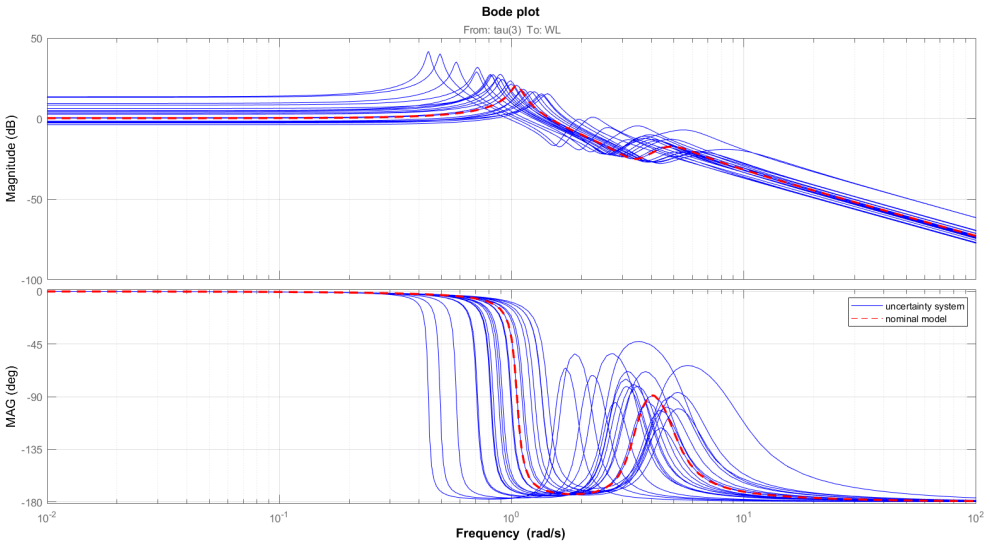

Figure 15: Bode plot from τ_3 to W_L

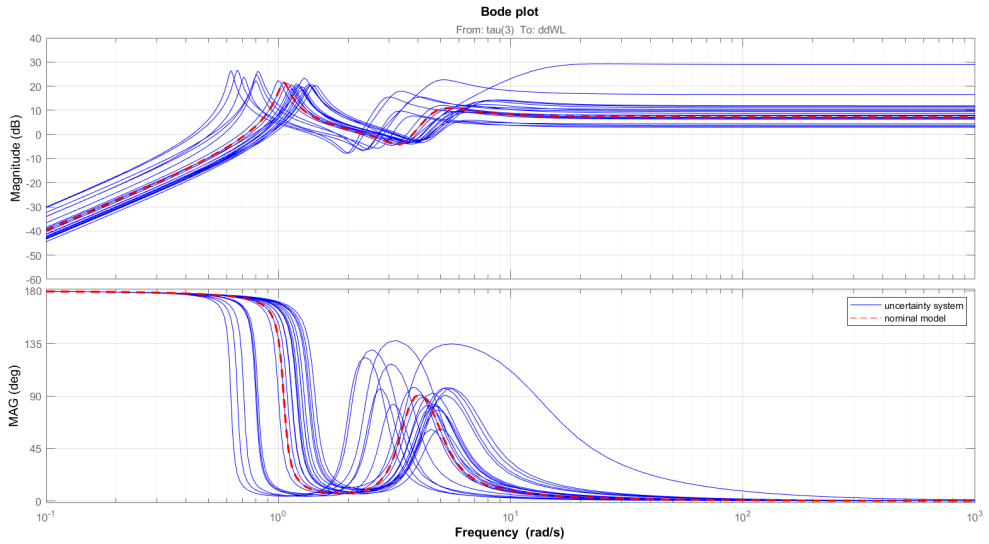

Figure 16: Bode plot from τ_3 to $\ddot{W}_L$

A torque signal was designed to act as a disturbance for plant G, in this case only τ_y and τ_z are excited as can be seen on figures 18 and 19.

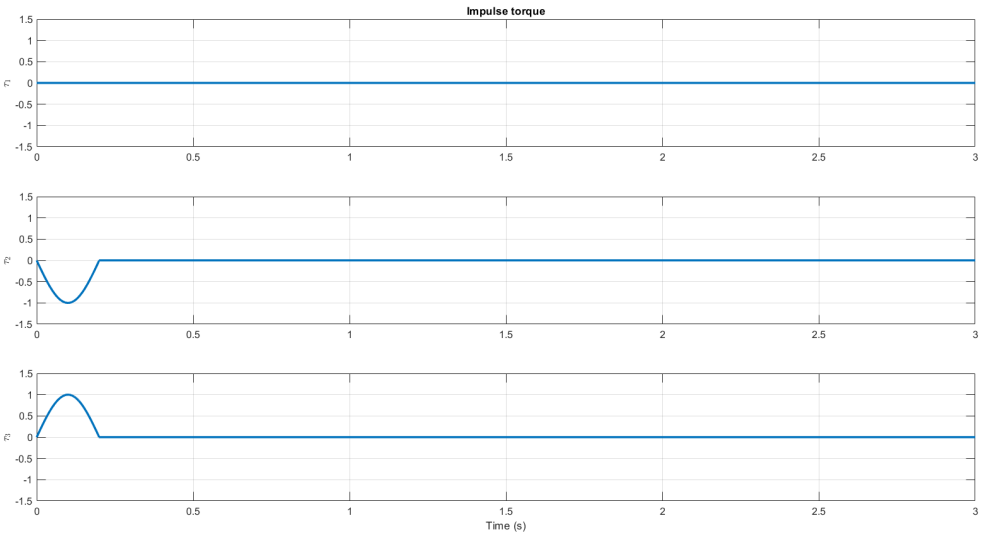

Figure 17: Impulse input torque

The impulse response of the system can be observed in figure 18:

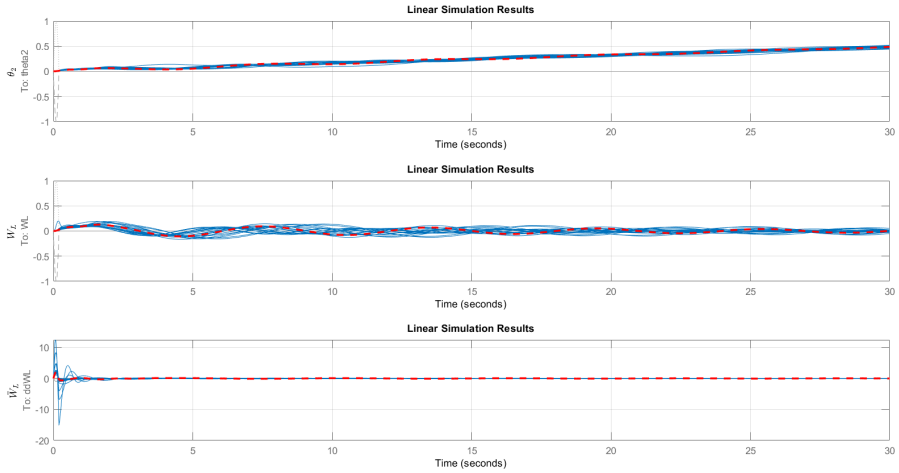

Figure 18: Impulse response of plant G for states θ_2, W_L and $\ddot{W}_L$

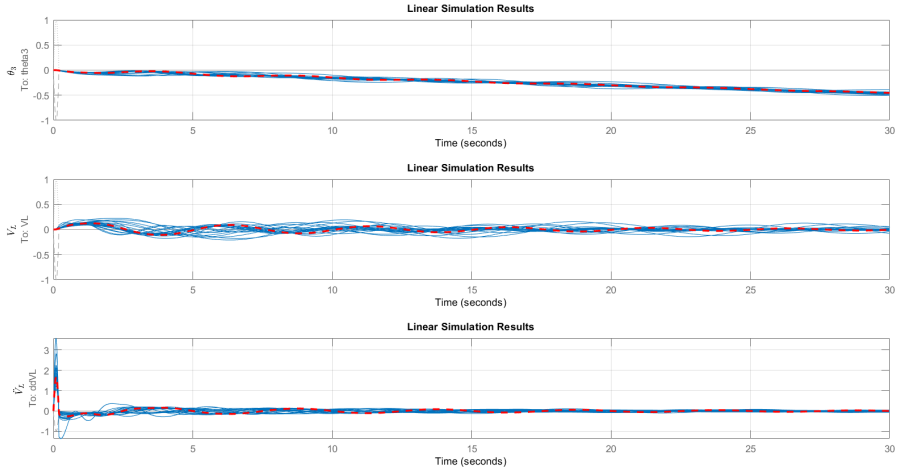

Figure 19: Impulse response of plant G for states θ_3, V_L and $\ddot{V}_L$

The states θ_2 and θ_3 in figure 18 and 19 respectively show an approximate linear increase through time due to the torque input disturbance, however is also important to note that this angle are wobbling. This is due to impact of the other states η_{1y}, η_{2y}, η_{1z} and η_{2z} indicating a dynamic relation between the flexible link and the rigid main satellite. A vibration suppression control is necessary not only to suppress the lateral displacements of the beam (w and v) but also to minimize its impact on the entire structure.

4 Control strategy and controller synthesis

The control strategy requires as sensor data the angular displacement in the three axis $(\theta_1, \theta_2, \theta_3)$ and the acceleration of the flexible appendage lateral deformation $(\ddot{V}$,$\ddot{W})$. Previous system interconnection in figure 9 is expressed as an integrated single block with torque vector as input and seven output signals, this new plant will be denoted by the letter G:

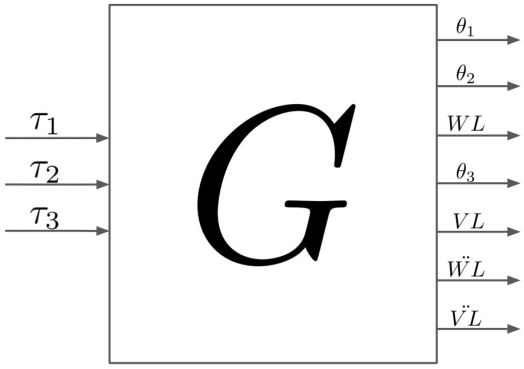

Figure 20: Integrated block diagram of Rigid-Flexible satellite system

For the design of an H_∞ controller the obtained G plant is interconnected with some new blocks:

- Actuators transfer function W_{a1}, W_{a2} and W_{a3} which are modeled as a first order lag with time constant 0.004 and gain 1.

- Plant performance weights W_{p1}, W_{p21}, W_{p22}, W_{p31} and W_{p32}. Their value will depend on what the controller must consider a priority. In this project the assigned weights for the desired orientation performance are greater than the rest, as a consequence desired orientation must be achieved first and then flexible appendage vibration can be suppressed, frequency response comparison between W_{p1} and W_{p22} can be observed in figure 21.

- Control performance weights W_{u1}, W_{u2} and W_{u3}. These scalar values denote how expensive or cheap the close loop system perceives control signal generation. If there are no restriction on how much torque can be generated, the value of these weights can be set very low.

- Noise shape filters W_{n1},W_{n21},W_{n22},W_{n31} and W_{n32}.Are determined according to the spectral contents of the sensor noises

- Reference dynamic models M_1, M_2, M_3, M_4 and M_5. These are not weighting functions but desired dynamic responses of the close loop plant when exited with a reference signal. The difference between the output of this blocks and the real states is what must be minimized by the robust controller.

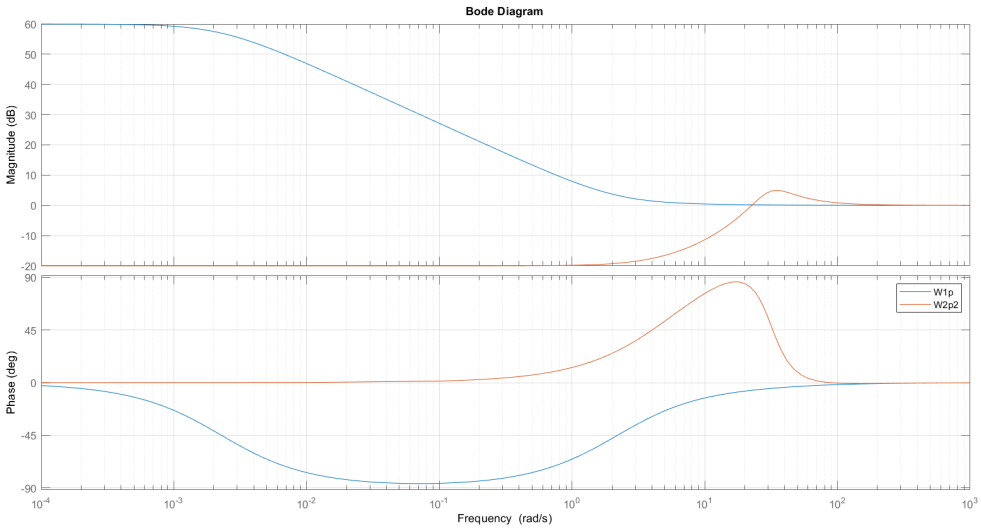

Figure 21: Bode plot comparison between W_{p1} and W_{p22}

Interconnected open loop plant can be observed in figure 22:

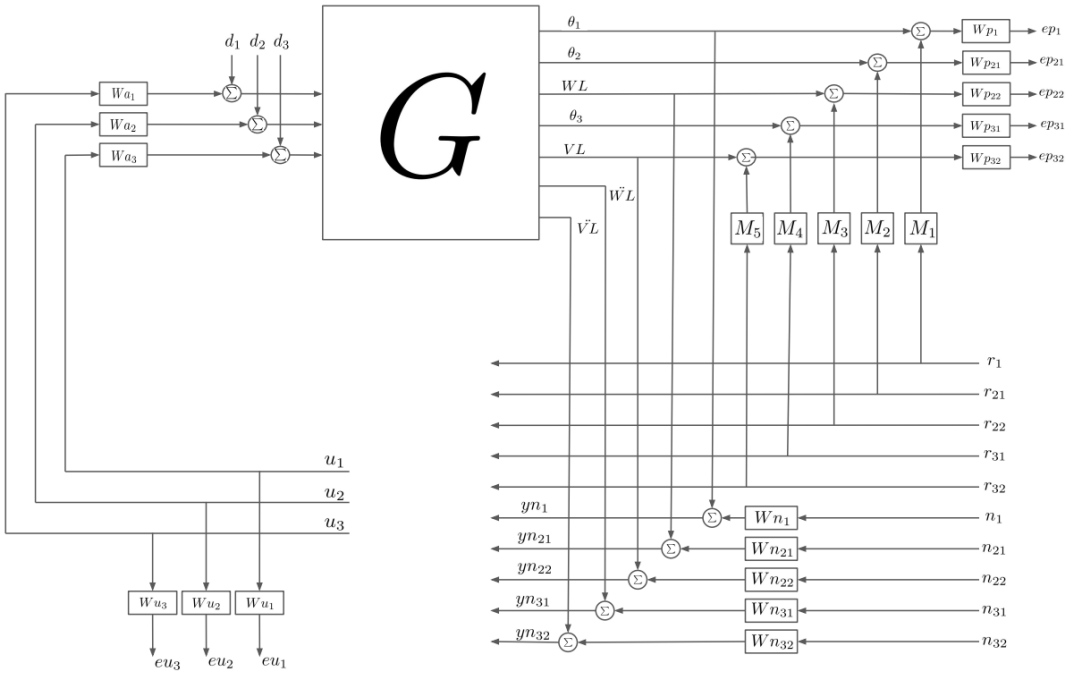

Figure 22: Open loop interconnection

Where inputs r, d, N and u refer to the reference signal, disturbance signal, noise and control input. The values of the system weights are defined as follow:

$$M_1 = M_2 = M3 = M_4 = M_5 = 1$$

$$W_{u1} = W_{u2} = W_{u3} = 0.001$$

$$W_{a1} = W_{a2} = W_{a3} = \frac{1}{0.004s+1}$$

$$W_{p1} = W_{p21} = W_{p31} = \frac{s^2+25s+50}{s^2+22s+0.05}$$

$$W_{p22} = W_{p32} = \frac{s^2+25s+100}{s^2+22s+1000}$$

$$W_{n1} = W_{n21} = W_{n31} = 10^{-5}\frac{0.5s+1}{0.005s+1}$$

$$W_{n22} = W_{n32} = 10^{-6}\frac{0.5s+1}{0.005s+1}$$

As mentioned in section 3.3 the main objective of a robust controller is to minimize the impact of the exogenous inputs $[r \quad d \quad n]$ into the regulated outputs [$ep1$, $ep21$, $ep22$, $ep31$ and $ep32$], close loop interconnection with the controller K is show in figure 23:

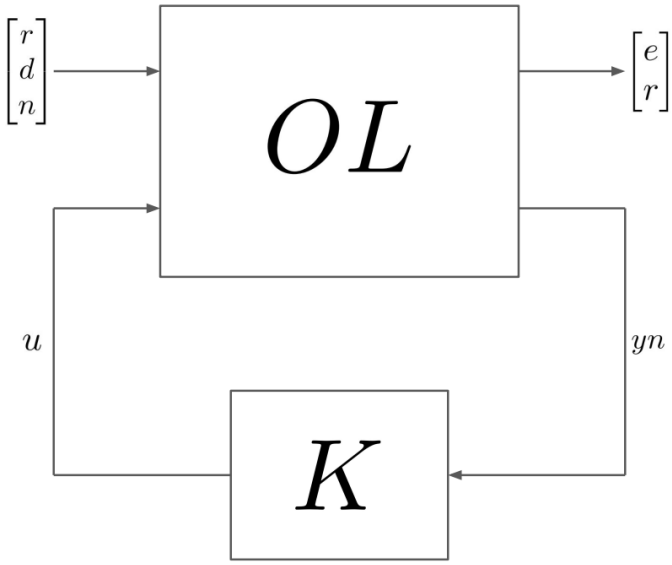

Figure 23: LFT representation of the open loop plant and the controller

Where OL is the integrated block of the open loop interconnection from figure 22:

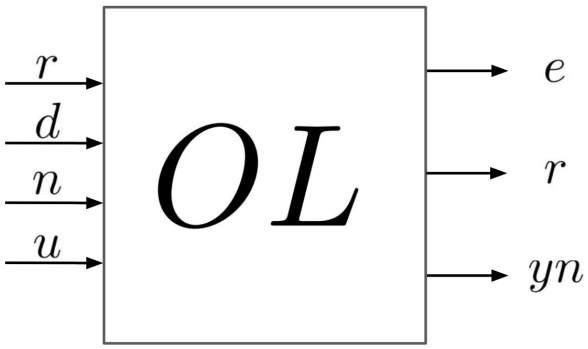

Figure 24: Integrated block diagram of the open loop system

The controller K is obtained by using the $hinf$ robust control synthesis command from the MATLAB robust control toolbox [50]. The obtained controller is interconnected with the nominal plant as shown on figure 25.

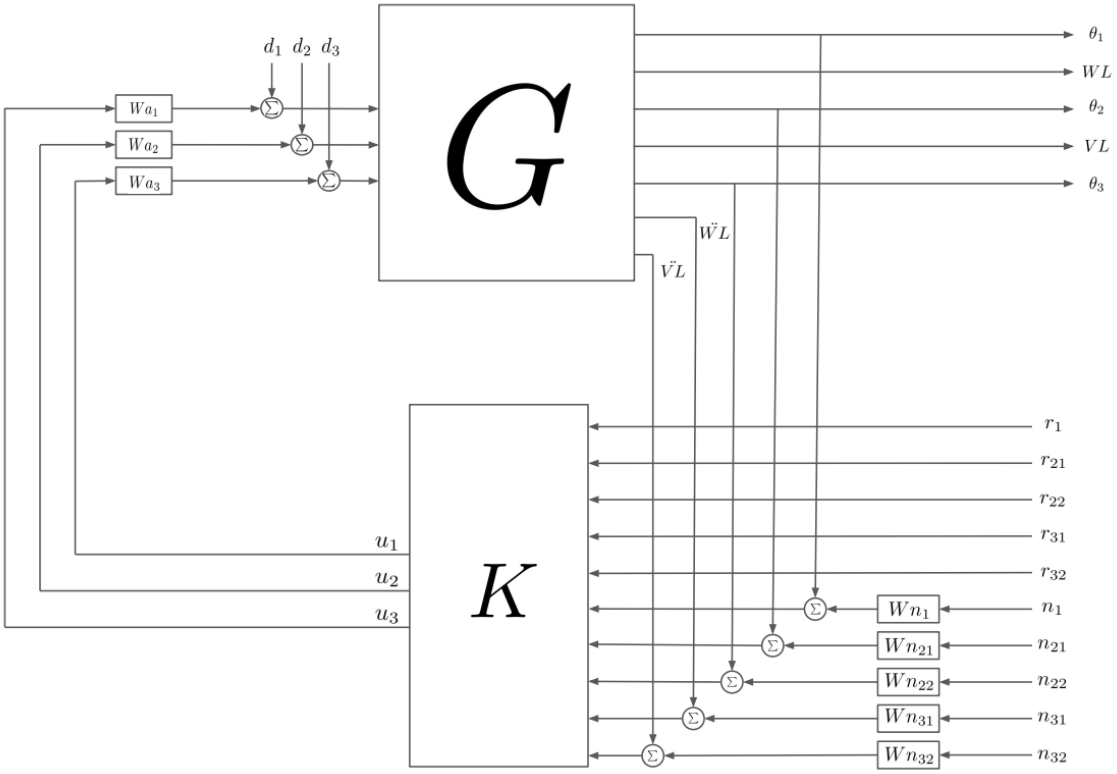

Figure 25: Close loop interconnection

5 Close loop system testing and Results

The desired reference angular orientation is $[20^o \ -15^o \ 10^0]$ for θ_1, θ_2 and θ_3 respectively. Objective orientation of the rigid main satellite must be achieved after 15 seconds. The error Euler angle plot in figure 26 shows that the close loop system is capable of reaching the objective orientation after approximately 18 seconds with an approximate error of 0.19^o, 0.25^o and 0.35^o after 30 seconds.

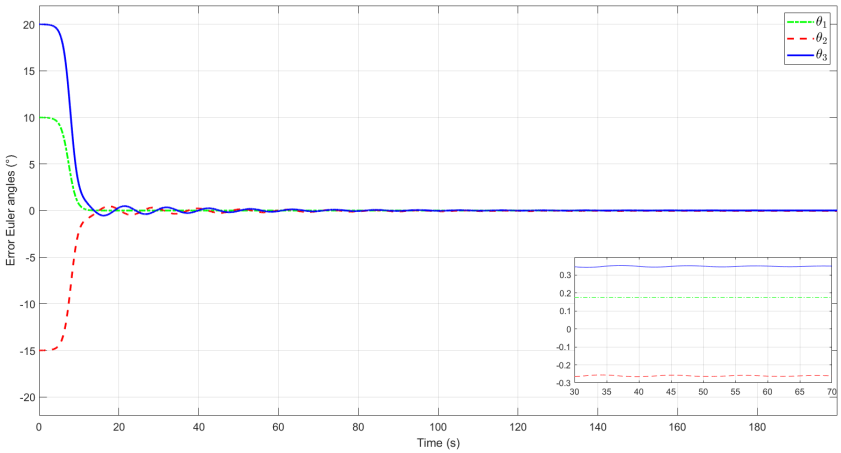

Figure 26: Error Euler angle using H_∞ control

Like it was stated before, the controller is focusing primarily on reaching the objective orientation as fastest as possible. Once the first task is completed the close loop plant starts dealing with the vibration suppression issue on V_L and W_L, these results can be observed in figures 27 and 28.

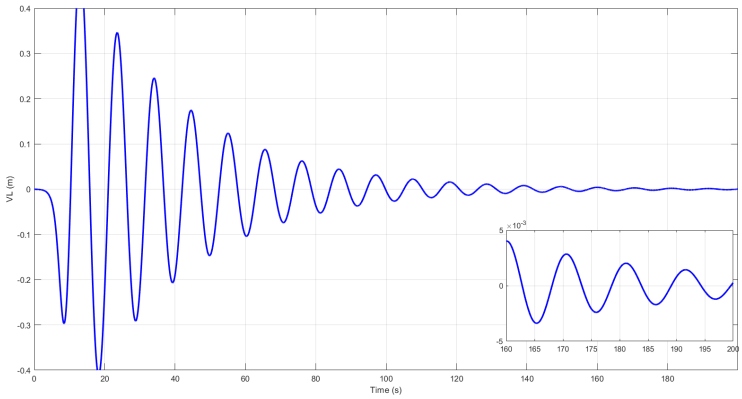

Figure 27: V_L vibration suppression using H_∞ control

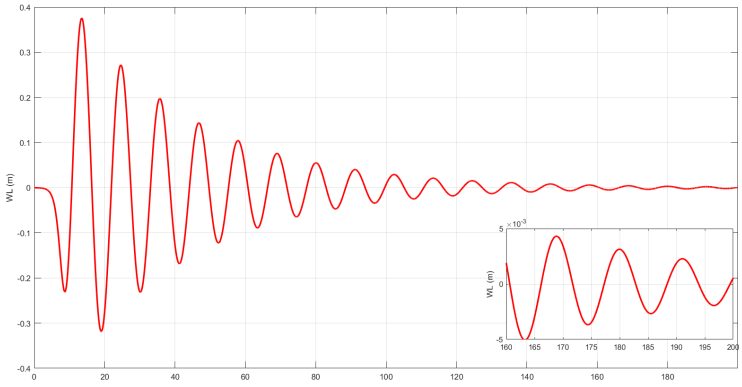

Figure 28: W_L vibration suppression using H_∞ control

As can be seen from these results, vibration is almost completely suppressed after approximately 160 seconds for both cases (V_L and W_L), since maximum vibration after this time instant is of five millimeters. Control input effort from the H_∞ controller can be observed in next figure:

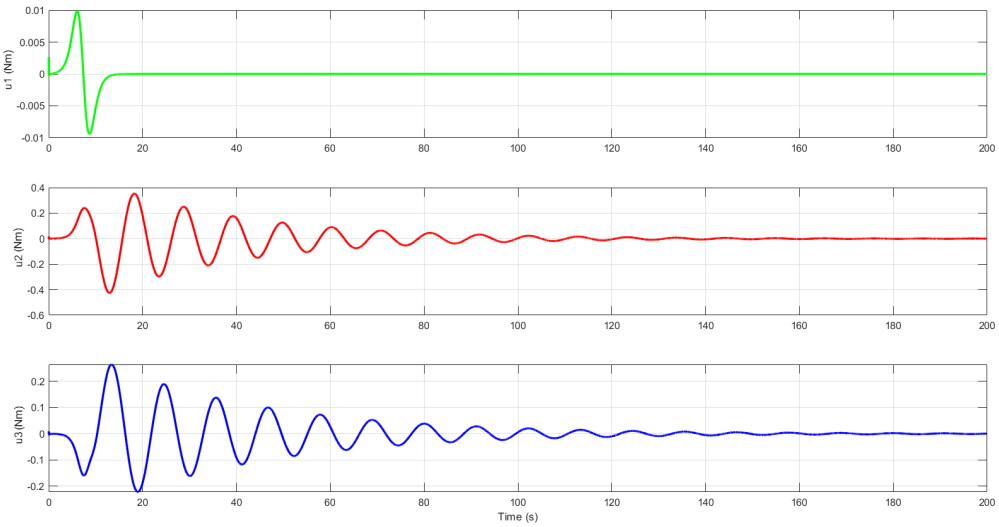

Figure 29: H_∞ control effort

It can be inferred that the designed H_∞ controller y capable of controlling the nominal plant of the system with almost no issues, since objective orientation and vibration suppression are achieved. Nevertheless, parametric uncertainty is always an important factor while testing the efficacy of a control system. The same H_∞ controller will now tested while considering the parametric uncertainty of the system.

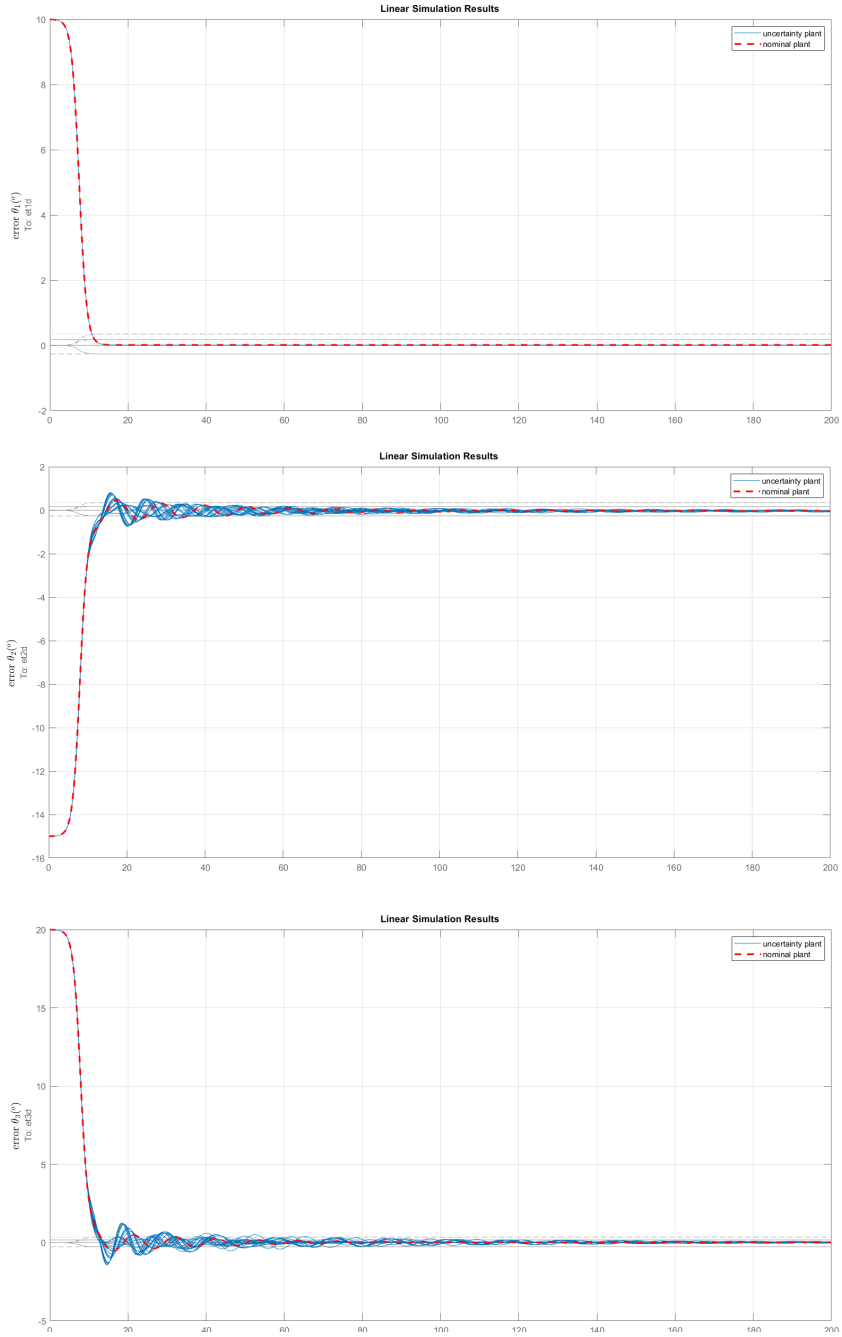

Figure 30: Error Euler angles using H_∞ control considering parametric uncertainty

From figure 30 it can be observed that parametric uncertainty mostly affect the Euler angles that are related to the respective lateral vibration of the flexible appendage ($\theta_2 \rightarrow W_L$ and $\theta_3 \rightarrow V_L$). Though it could be perceived that all Euler angles will converge to the objective orientation, the time required for this is too large. Also, vibration at the tip is not in a better situation since, as can be seen on figures 31 and 32, lateral deformation after 160 seconds is not even lees than 0.08 and 0.22 meters for W_L and V_L respectively.

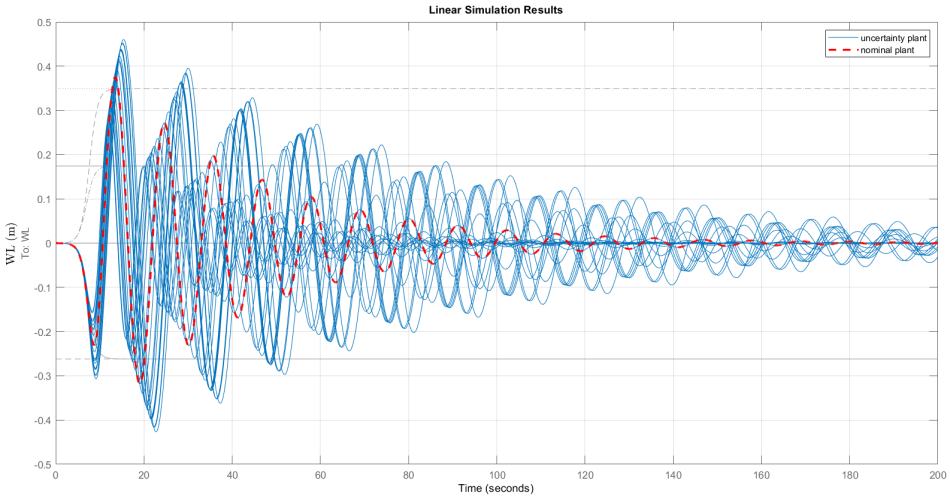

Figure 31: W_L vibration suppression using H_∞ control considering parametric uncertainty

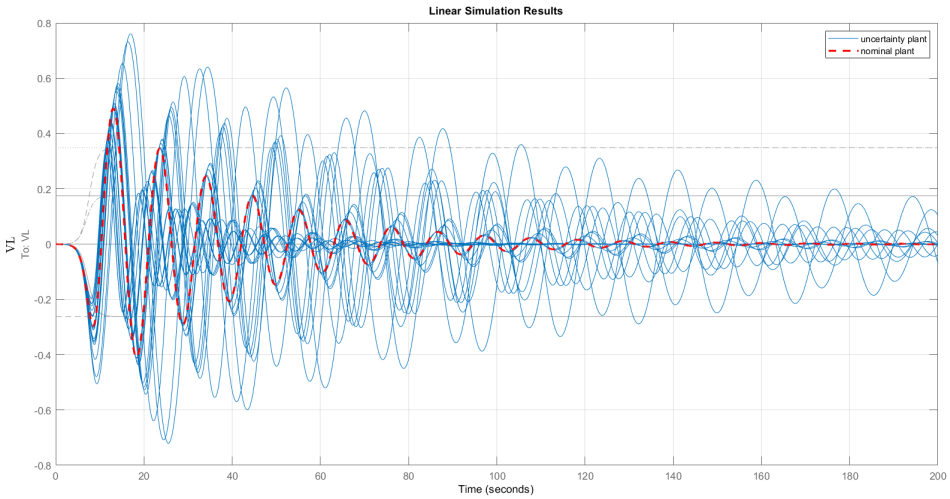

Figure 32: V_L vibration suppression using H_∞ control considering parametric uncertainty

The obtained H_∞ controller is not robust enough to deal with large parametric uncertainties, as a consequence a more robust controller is required. To address this issue the μ control synthesis will be used to obtain a more robust controller that can keep good performance while dealing with parametric uncertainties. The $musyn$ command from MATLAB robust control toolbox is used to synthesize a more robust controller that will be tested in the same way as in the previous case. The Euler angle errors of the nominal plant controlled by the μ controller can be observe in figure 33.

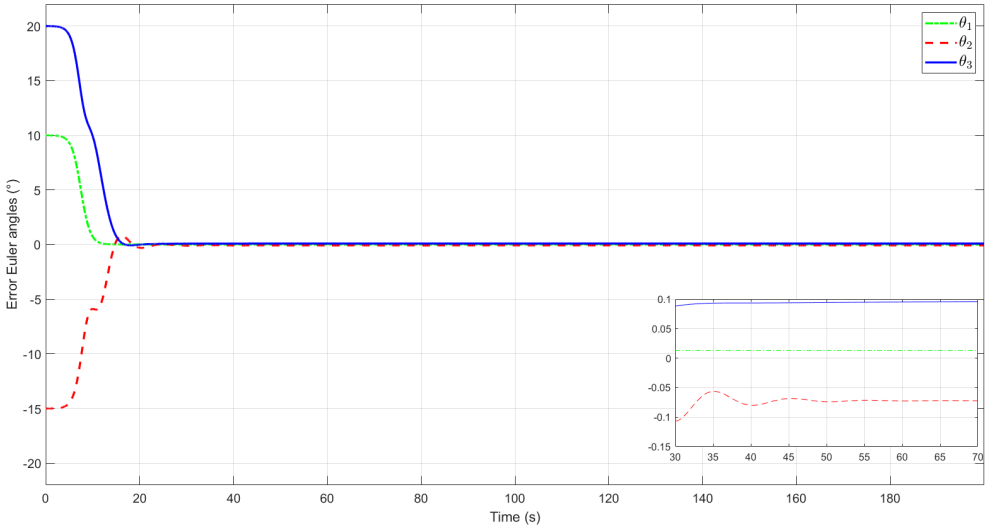

Figure 33: Error Euler angle using μ synthesis control

The desired orientation is reached approximately after 18 seconds with an approximate error of 0.01^o, 0.06^o and 0.09^o for Euler angles θ_1, θ_2 and θ_3 respectively after 30 seconds. Vibration on the nominal plant is suppressed in a more efficient way if compared to the H_∞ controller, this can be seen on figures 34 and 35.

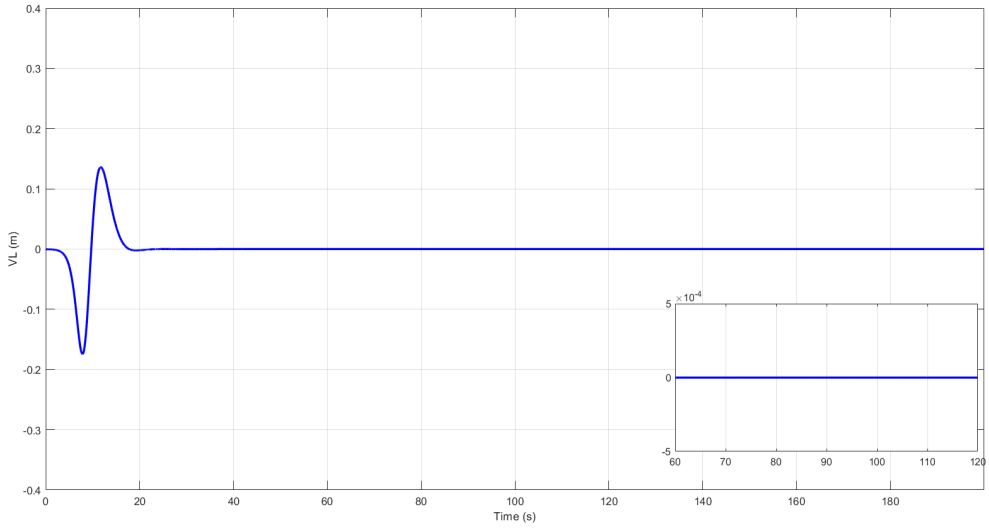

Figure 34: V_L vibration suppression using μ synthesis control

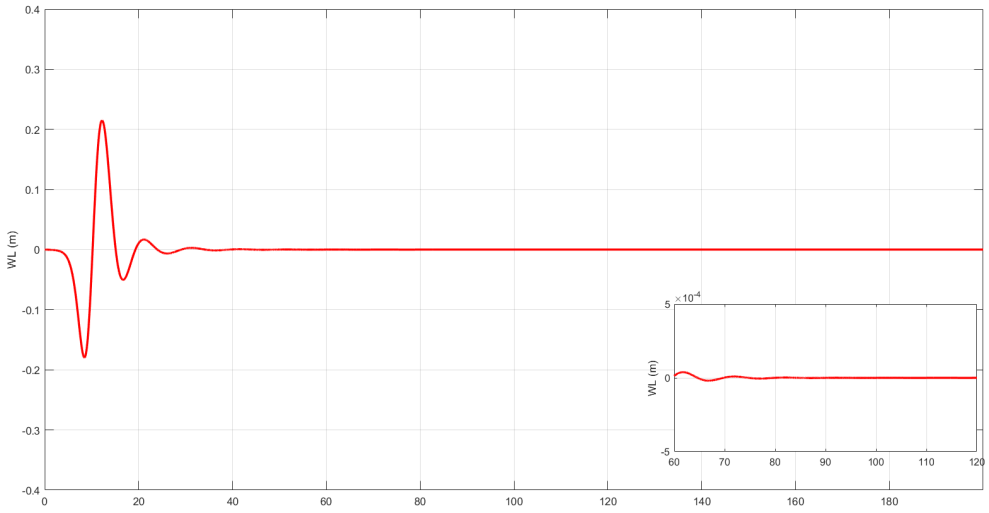

Figure 35: W_L vibration suppression using μ synthesis control

Control input effort from the μ controller can be observed in next figure:

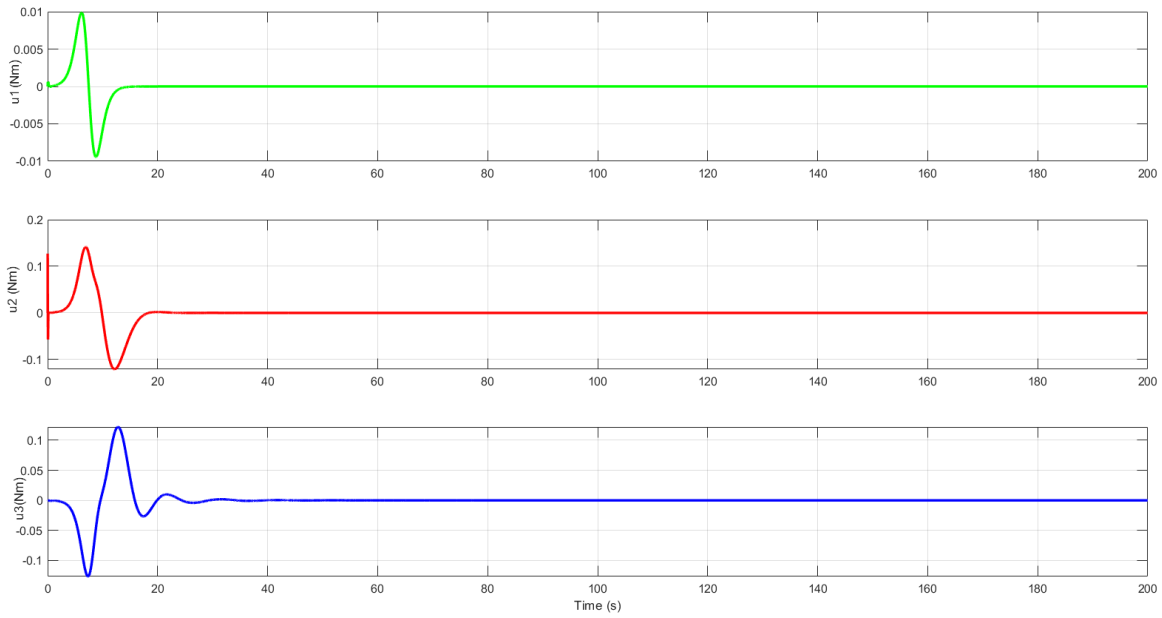

Figure 36: μ synthesis control effort

The close-loop plant using the μ controller will be tested considering the parametric uncertainty. The error Euler angles can be observed in figure 37, when these results are compared to the ones at 30 it can be concluded that the μ controller can achieve much better results under the influence of parametric uncertainty.

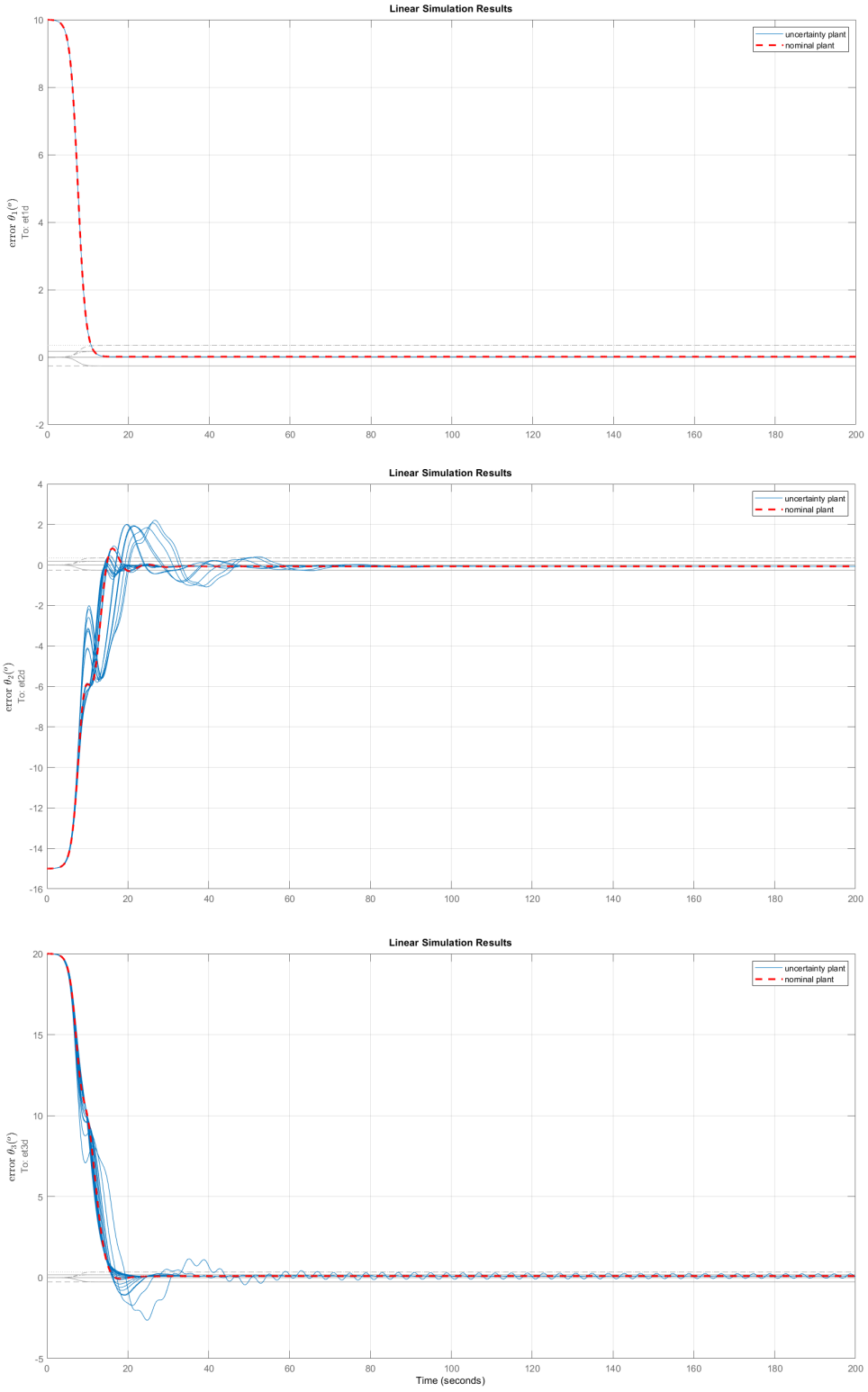

Figure 37: Error Euler angles using μ synthesis control considering uncertainty

Vibration suppression results at figures 38 and 39 show that the μ controller can guarantee stability, aspect that was not achieved by the previous H_∞ controller. A closer look to these results can be observed at figures 40 and 41, where it is possible to notice that after 60 seconds vibration is less than two and ten millimeters for W_L and V_L respectively.

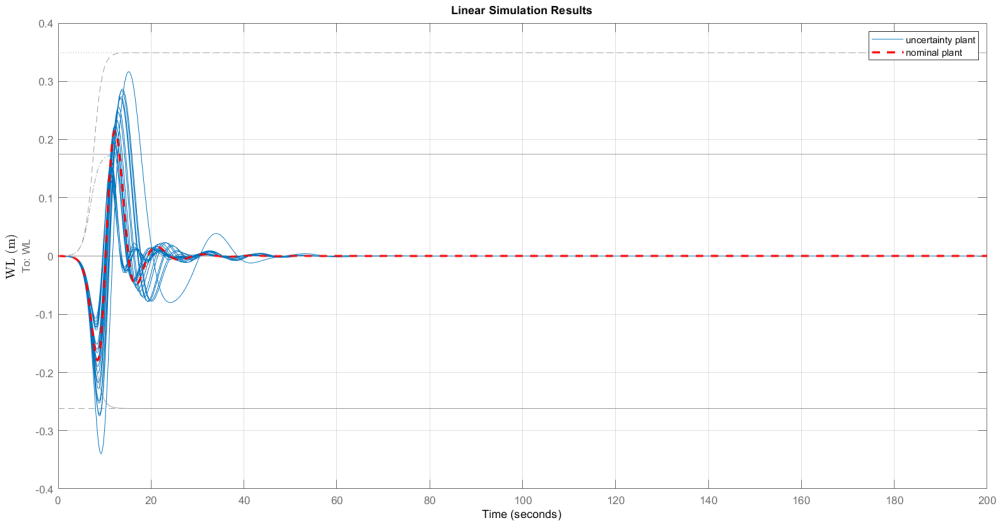

Figure 38: W_L vibration suppression using μ synthesis control considering uncertainty

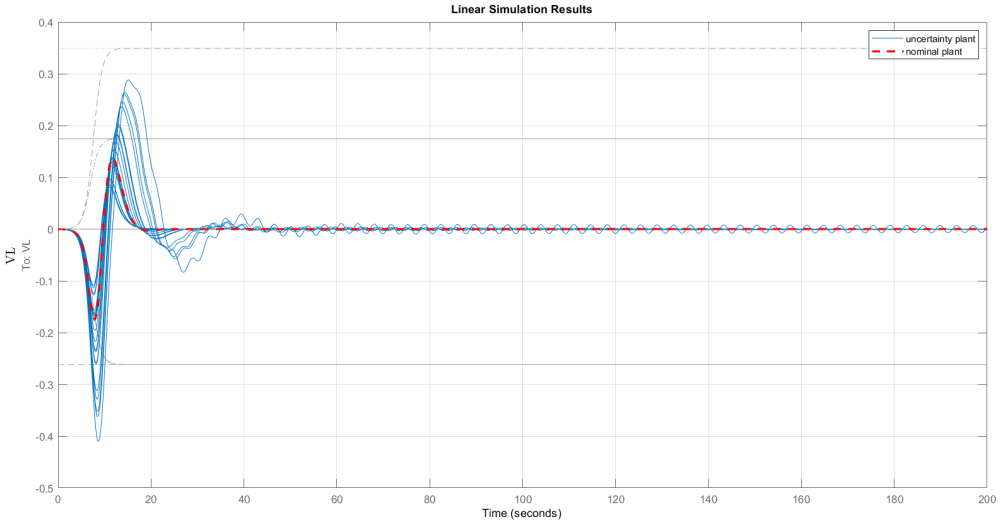

Figure 39: V_L vibration suppression using μ synthesis control considering uncertainty

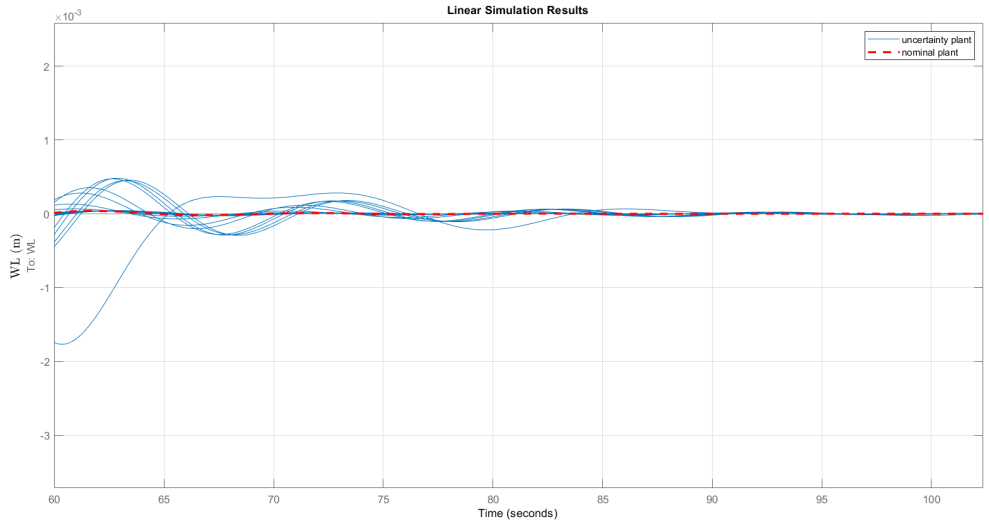

Figure 40: W_L vibration suppression using μ synthesis control considering uncertainty

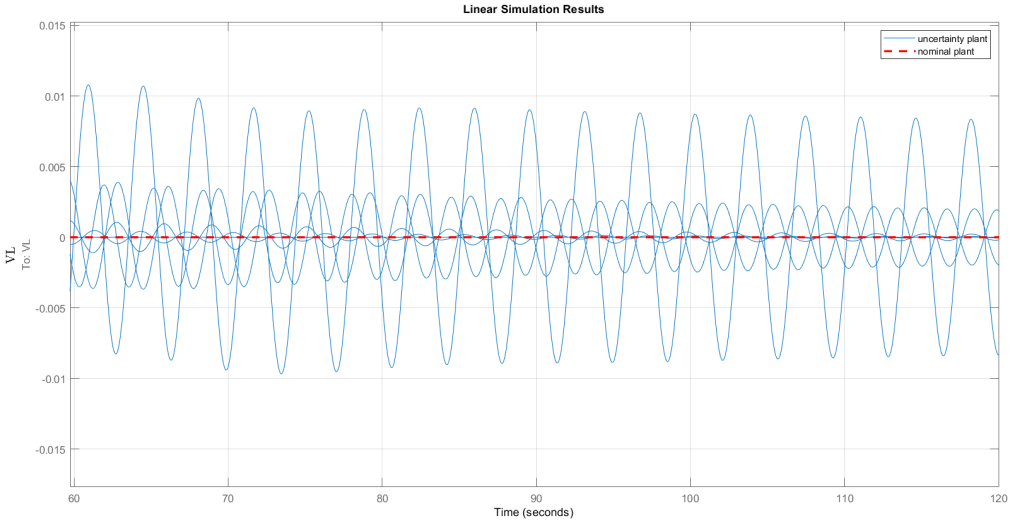

Figure 41: V_L vibration suppression using μ synthesis control considering uncertainty

Conclusions and future work

The dynamic modeling of a rigid flexible satellite was obtained, the Lagrangian method was used to obtain the equations of motion of the system, then these were discretized by using the assumed modes method. The discretized equation of motion was linearized and a plant G with parametric uncertainty was created.

An open loop plant of the modeled system was interconnected with the weighting functions in order to compute a robust controller. The obtained controller was designed to firstly focus on reaching the desired orientation, vibration suppression was second in priority, this was defined by the weighting functions in section 4.

The first proposed controller used the H_∞ synthesis to compute a K that could control and stabilize the system. The obtained controller was capable of reaching the desired orientation in a short period of time and suppress flexible appendage vibration after a period of 160 seconds. Nevertheless when tested under the presence of parametric uncertainty the controller was not capable of stabilizing the plant fast enough by itself.

In order to guarantee fast converge of the system under the presence of parametric uncertainty a μ synthesis controller was derived. In contrast to previous H_∞ technique, the μ synthesis considers the parametric uncertainty while computing a valid controller that can deal with this issue. The obtained K was not only capable of reaching the desired orientation, but also it was capable of suppressing the flexible appendage vibration after a short period of time while dealing with an uncertain plant.

Plant linearization around an equilibrium point is useful at the moment of deriving a linear controller such as H_∞ or μ. Unfortunately a non-linearized plan will be always closer to a real system than a linearized one, due to this a non-linear controller and a adaptive controller are proposed as a future task, results must be compared with the ones obtained in this report.

Validation of the obtained dynamics will be addressed. The same structure of this project must be modeled on a FEM specialize software such as ANSYS or SimScape.

References

[1] Z. Xu, Y. Guannan, H. Hai, and W. Xinsheng. Deployment analysis and test of a coilable mast for buaa student micro-satellite[A]. 2010 3rd International Symposium on Systems and Control in Aeronautics and Astronautics [C]. IEEE, 2010, pp. 1329-1332.

[2] L. Fan, H. Huang, L. Sun, and K. Zhou. Robust attitude control for a rigid-flexible-rigid microsatellite with multiple uncertainties and input saturations [J]. Aerospace Science and Technology, vol. 95, p. 105443, 2019.

[3] V. Modi. Attitude dynamics of satellites with flexible appendages-a brief review [J]. Journal of Spacecraft and Rockets, vol. 11, no. 11, pp. 743-751, 1974.

[4] M. Schenk, A. D. Viquerat, K. A. Seffen, and S. D. Guest. Review of inflatable booms for deployable space structures: packing and rigidization [J]. Journal of Spacecraft and Rockets, vol. 51, no. 3, pp. 762-778, 2014.

[5] A. Cornogolub, New technique for deploying long coilable booms, without blossoming effect, using a polymer joint [J]. IFAC-PapersOnLine, vol. 52, no. 12, pp. 555-559,2019.

[6] Z. You. Space Microsystems and Micro-Nano Satellites. Butterworth-Heinemann. 2017.

[7] F. L. Markley and J. L. Crassidis. Fundamentals of spacecraft attitude determination and control. Springer. 2014, vol. 33.

[8] M. L. Tibbs, Design and test of an attitude determination and control system for a 6u cubesat using afit's cubesat testbed. 2015

[9] M. Vos, Delfi-n3xt's attitude determiniation and control subsystem: Implementation and verification of the hardware and software. Master's thesis, Delft University of Technology, 2013.

[10] D. Torczynski, R. Amini, and P. Massioni, Magnetorquer based attitude control for a nanosatellite testplatform [A]. AIAA Infotech@ Aerospace 2010 [C], 2010, p. 3511.

[11] M. Prinkey. Cubesat attitude control testbed design: Merritt 4-coil per axis helmholtz cage and spherical air bearing [A].AIAA Guidance, Navigation, and Control (GNC) Con- ference [C]. 2013, p. 4942.

[12] M. K. Quadrino. Testing the attitude determination and control of a cubesat with hardware-in-the-loop. Master's thesis, Massachusetts Institute of Technology, 2014.

[13] W. Blackwell, G. Allen, C. Galbraith, R. Leslie, I. Osaretin, M. Scarito, M. Shields, E. Thompson, D. Toher, D. Townzen et al. Micromas: A first step towards a nanosatellite constellation for global storm observation. 2013.

[14] T. Nguyen, K. Cahoy, and A. Marinan. Attitude determination for small satellites with infrared earth horizon sensors [J]. Journal of Spacecraft and Rockets, vol. 55, no. 6, pp. 1466-1475, 2018.

[15] J. Yang, L. Jiang, and D. C. Chen. Dynamic modeling and control of a rotating euler-bernoulli beam [J]. Journal of sound and vibration, vol. 274, no. 3-5, pp. 863-875, 2004.

[16] S. S. Ge, S. Zhang, and W. He. Modeling and control of an euler-bernoulli beam under unknown spatiotemporally varying disturbance [A]. Proceedings of the 2011 American Control Conference [C]. IEEE, 2011, pp. 2988-2993.

[17] W. Manning, A. R. Plummer, and M. Levesley. Vibration control of a flexible beam with integrated actuators and sensors [J]. Smart Materials and Structures, vol. 9, no. 6, p. 932, 2000.

[18] W. Zhu and C. Mote Jr. Dynamic modeling and optimal control of rotating euler-bernoulli beams. 1997.

[19] D. Sun and J. K. Mills. Control of a rotating cantilever beam using a torque actuator and a distributed piezoelectric polymer actuator [J]. Applied Acoustics, vol. 63, no. 8, pp. 885-899, 2002.

[20] S. Choura, S. Jayasuriya, and M. A. Medick. On the modeling, and open-loop control of a rotating thin flexible beam. 1991.

[21] S. Hoa. Vibration of a rotating beam with tip mass [J]. Journal of sound and vibration, vol. 67, no. 3, pp. 369-381, 1979.

[22] H. Yang, J. Hong, and Z. Yu. Dynamics modelling of a flexible hub-beam system with a tip mass [J]. Journal of Sound and Vibration, vol. 266, no. 4, pp. 759-774, 2003.

[23] S. Y. Lee, S. M. Lin, and C. T. Wu. Free vibration of a rotating non-uniform beam with arbitrary pretwist, an elastically restrained root and a tip mass [J]. Journal of Sound and Vibration, vol. 273, no. 3, pp. 477-492, 2004.

[24] S. Bai, P. Ben-Tzvi, Q. Zhou, and X. Huang. Dynamic modeling of a rotating beam having a tip mass [A]. in 2008 International Workshop on Robotic and Sensors Environments [C]. IEEE, 2008, pp. 52-57.

[25] D. Zhang, J. Liu, J. Huang, and W. Zhu. Periodic responses of a rotating hub-beam system with a tip mass under gravity loads by the incremental harmonic balance method [J]. Shock and Vibration, vol. 2018, 2018.

[26] H. H. Yoo, S. Seo. and K. Huh. The effect of a concentrated mass on the modal characteristics of a rotating cantilever beam [J]. Proceedings of the Institution of Mechanical Engineers, Part C: Journal of Mechanical Engineering Science, vol. 216, no. 2, pp. 151-163, 2002.

[27] J. L. Redondo Gutierrez. Attitude control of flexible spacecraft: Design, implementation and evaluation of control strategies targeting flexible structures in the space domain, based in an analytical modeling of these structures. 2019.

[28] K. Lips and V. Modi. General dynamics of a large class of flexible satellite systems [J]. Acta Astronautica, vol. 7, no. 12, pp. 1349-1360, 1980.

[29] A. De Souza and L. De Souza. H infinity controller design to a rigid-flexible satellite with two vibration modes [J]. Journal of Physics: Conference Series, vol. 641, no. 1. IOP Publishing, 2015, p. 012030.

[30] A. Souza and L. Souza. Design of a controller for a rigid-flexible satellite using the h-infinity method considering the parametric uncertainty [J]. Mechanical Systems and Signal Processing, vol. 116, pp. 641-650, 2019.

[31] W. He and S. S. Ge. Dynamic modeling and vibration control of a flexible satellite [J]. IEEE Transactions on Aerospace and Electronic Systems, vol. 51, no. 2, pp. 1422-1431, 2015.

[32] H. Liu, L. Guo, and Y. Zhang. An anti-disturbance PD control scheme for attitude control and stabilization of flexible spacecrafts [J]. Nonlinear Dynamics, vol. 67, no. 3, pp. 2081- 2088, 2012.

[33] L. Guo and W.-H. Chen. Disturbance attenuation and rejection for systems with nonlinear-ity via dobc approach [J]. International Journal of Robust and Nonlinear Control: IFAC-Affiliated Journal, vol. 15, no. 3, pp. 109-125, 2005.

[34] S. Wu, W. Chu, X. Ma, G. Radice, and Z. Wu, Multi-objective integrated robust H_∞ control for attitude tracking of a flexible spacecraft [J]. Acta Astronautica, vol. 151, pp. 80-87, 2018.

[35] L. Liu and D. Cao. Dynamic modeling for a flexible spacecraft with solar arrays composed of honeycomb panels and its proportional-derivative control with input shaper [J]. Journal of Dynamic Systems, Measurement, and Control, vol. 138, no. 8, 2016.

[36] K. W. Lee and S. N. Singh. L1 adaptive control of flexible spacecraft despite disturbances [J]. Acta Astronautica, vol. 80, pp. 24-35, 2012.

[37] N. Hovakimyan and C. Cao. L1 Adaptive Control Theory: Guaranteed Robustness with Fast Adaptation. SIAM, 2010.

[38] Z. Qinghua, M. Guangfu, W. Xiaoting, and W. Aiguo. Attitude control without angular velocity measurement for flexible satellites [J]. Chinese Journal of Aeronautics, vol. 31, no. 6, pp. 1345-1351, 2018.

[39] V. L. Pisacane. The space environment and its effects on space systems. American Institute of aeronautics and Astronautics. 2008.

[40] D. A. Vallado. Fundamentals of astrodynamics and applications. Springer Science and Business Media, 2001, vol. 12.

[41] J. L. Junkins and Y. Kim. Introduction to dynamics and control of flexible structures. American Institute of Aeronautics and Astronautics, 1993.

[42] L. Mazzini, Flexible Spacecraft Dynamics, Control and Guidance. Springer, 2015.

[43] A. Preumont, Vibration control of active structures. Springer, 1997, vol. 2.

[44] R. J. Theodore and A. Ghosal. Comparison of the assumed modes and finite element mod- els for flexible multilink manipulators [J]. The International journal of robotics research, vol. 14, no. 2, pp. 91-111, 1995.

[45] M. G. Safonov. Origins of robust control: Early history and future speculations [J]. Annual Reviews in Control, vol. 36, no. 2, pp. 173-181, 2012.

[46] D.-W. Gu, P. Petkov, and M. M. Konstantinov. Robust control design with MATLAB®R . Springer Science and Business Media, 2005.

[47] S. Boyd, L. El Ghaoui, E. Feron, and V. Balakrishnan. Linear matrix inequalities in system and control theory. SIAM, 1994.

[48] G.-R. Duan and H.-H. Yu. LMIs in control systems: analysis, design and applications. CRC press, 2013.

[49] C. M. Belcastro. Parametric uncertainty modeling: an overview [A]. Proceedings of the 1998 American Control Conference [C]. ACC (IEEE Cat. No. 98CH36207), vol. 2. IEEE, 1998, pp. 992-996.

[50] G. Balas, R. Chiang, A. Packard, and M. Safonov, Robust control toolbox user's guide," The Math Works, Inc., Tech. Rep, 2007.

Acknowledgments

My gratitude go first to my beloved mother and father, their unconditional love is by far the most important factor on my everyday progression to reach my dreams and objectives. The charisma and brotherhood of my dear sister and brother were there also to comfort me, mostly on those times of uncertainty and fatigue. Also I want to thank my grand mother and my aunt who everyday showed how worried and proud they were about me.

I want to express my gratitude to professor Eber Huanca, from Universidad Catolica San Pablo, who taught me how to work on a team and showed me how to maintain hope even during the most complicated moments.

Thanks to CONIDA and APSCO for giving me the opportunity to study my master degree and for investing in my professional development . Thanks BUAA for pushing me to learn more by myself, and finally I want to express my gratitude to the international school which taught to depend less on others.